



U.S. Department of
Transportation

**Federal Railroad
Administration**

Blunt Impact Testing of a Diesel Multiple Unit Fuel Tank

Office of Research,
Development
and Technology
Washington, DC 20590



NOTICE

This document is disseminated under the sponsorship of the Department of Transportation in the interest of information exchange. The United States Government assumes no liability for its contents or use thereof. Any opinions, findings and conclusions, or recommendations expressed in this material do not necessarily reflect the views or policies of the United States Government, nor does mention of trade names, commercial products, or organizations imply endorsement by the United States Government. The United States Government assumes no liability for the content or use of the material contained in this document.

NOTICE

The United States Government does not endorse products or manufacturers. Trade or manufacturers' names appear herein solely because they are considered essential to the objective of this report.

REPORT DOCUMENTATION PAGEForm Approved
OMB No. 0704-0188

Public reporting burden for this collection of information is estimated to average 1 hour per response, including the time for reviewing instructions, searching existing data sources, gathering and maintaining the data needed, and completing and reviewing the collection of information. Send comments regarding this burden estimate or any other aspect of this collection of information, including suggestions for reducing this burden, to Washington Headquarters Services, Directorate for Information Operations and Reports, 1215 Jefferson Davis Highway, Suite 1204, Arlington, VA 22202-4302, and to the Office of Management and Budget, Paperwork Reduction Project (0704-0188), Washington, DC 20503.

1. AGENCY USE ONLY (Leave blank)		2. REPORT DATE July 2018	3. REPORT TYPE AND DATES COVERED Technical Report	
4. TITLE AND SUBTITLE Blunt Impact Testing of a Diesel Multiple Unit Fuel Tank			5. FUNDING NUMBERS DTFR5311D00008L Task Order 305	
6. AUTHOR(S) Travis Gorhum ¹ , Michael Carolan ² , Przemyslaw Rakoczy ¹ , Karina Jacobsen ² , Shaun Eshraghi ² , Melissa Shurland			8. PERFORMING ORGANIZATION REPORT NUMBER	
7. PERFORMING ORGANIZATION NAME(S) AND ADDRESS(ES) ¹ Transportation Technology Center, Inc., 55500 DOT Road, Pueblo, CO 81001 ² Volpe National Transportation Systems Center, 55 Broadway, Cambridge, MA 02142			10. SPONSORING/MONITORING AGENCY REPORT NUMBER DOT/FRA/ORD-18/22	
9. SPONSORING/MONITORING AGENCY NAME(S) AND ADDRESS(ES) U.S. Department of Transportation Federal Railroad Administration Office of Railroad Policy and Development Office of Research, Development and Technology Washington, DC 20590			11. SUPPLEMENTARY NOTES COR: Melissa Shurland	
12a. DISTRIBUTION/AVAILABILITY STATEMENT This document is available to the public through the FRA Web site at http://www.fra.dot.gov .			12b. DISTRIBUTION CODE	
13. ABSTRACT (Maximum 200 words) Transportation Technology Center, Inc. (TTCI) performed a dynamic impact test of a diesel multiple unit (DMU) fuel tank at the Transportation Technology Center (TTC) in Pueblo, CO, where an impact vehicle weighing approximately 14,000 pounds equipped with a rigid 12-inch by 12-inch impactor head struck the bottom surface of a DMU fuel tank. At 11.2 mph, the impactor struck the target area, centered over two internal baffles. The test resulted in a maximum indentation of approximately 8 inches. Following the test, TTC cut the fuel tank open to inspect the damage to the tank's internal structure. This revealed that several internal baffles in the surrounding area of the impact location buckled. The John A. Volpe National Transportation Systems Center developed the pre-test finite element (FE) model of the DMU fuel tank and impactor. Prior to the test, engineering drawings and computer-aided design (CAD) geometry were used to generate a detailed FE mesh of the fuel tank. The pre-test FE model was used to plan for instrumentation range and placement, as well as to estimate the desired test speed. The FE models of the fuel tank and the actual test results were in agreement. FRA can now use the validated FE model to simulate other impact scenarios of this fuel tank.				
14. SUBJECT TERMS Diesel multiple unit, DMU, fuel tanks, impact test, crashworthiness, finite element analysis, FEA, puncture resistance, passenger locomotive, fuel tanks			15. NUMBER OF PAGES 74	
			16. PRICE CODE	
17. SECURITY CLASSIFICATION OF REPORT Unclassified	18. SECURITY CLASSIFICATION OF THIS PAGE Unclassified	19. SECURITY CLASSIFICATION OF ABSTRACT Unclassified	20. LIMITATION OF ABSTRACT	

NSN 7540-01-280-5500

Standard Form 298 (Rev. 2-89)
Prescribed by ANSI Std. Z39-18
298-102

METRIC/ENGLISH CONVERSION FACTORS

ENGLISH TO METRIC

LENGTH (APPROXIMATE)

1 inch (in)	=	2.5 centimeters (cm)
1 foot (ft)	=	30 centimeters (cm)
1 yard (yd)	=	0.9 meter (m)
1 mile (mi)	=	1.6 kilometers (km)

AREA (APPROXIMATE)

1 square inch (sq in, in ²)	=	6.5 square centimeters (cm ²)
1 square foot (sq ft, ft ²)	=	0.09 square meter (m ²)
1 square yard (sq yd, yd ²)	=	0.8 square meter (m ²)
1 square mile (sq mi, mi ²)	=	2.6 square kilometers (km ²)
1 acre = 0.4 hectare (he)	=	4,000 square meters (m ²)

MASS - WEIGHT (APPROXIMATE)

1 ounce (oz)	=	28 grams (gm)
1 pound (lb)	=	0.45 kilogram (kg)
1 short ton = 2,000 pounds (lb)	=	0.9 tonne (t)

VOLUME (APPROXIMATE)

1 teaspoon (tsp)	=	5 milliliters (ml)
1 tablespoon (tbsp)	=	15 milliliters (ml)
1 fluid ounce (fl oz)	=	30 milliliters (ml)
1 cup (c)	=	0.24 liter (l)
1 pint (pt)	=	0.47 liter (l)
1 quart (qt)	=	0.96 liter (l)
1 gallon (gal)	=	3.8 liters (l)
1 cubic foot (cu ft, ft ³)	=	0.03 cubic meter (m ³)
1 cubic yard (cu yd, yd ³)	=	0.76 cubic meter (m ³)

TEMPERATURE (EXACT)

$$[(x-32)(5/9)] \text{ } ^\circ\text{F} = y \text{ } ^\circ\text{C}$$

METRIC TO ENGLISH

LENGTH (APPROXIMATE)

1 millimeter (mm)	=	0.04 inch (in)
1 centimeter (cm)	=	0.4 inch (in)
1 meter (m)	=	3.3 feet (ft)
1 meter (m)	=	1.1 yards (yd)
1 kilometer (km)	=	0.6 mile (mi)

AREA (APPROXIMATE)

1 square centimeter (cm ²)	=	0.16 square inch (sq in, in ²)
1 square meter (m ²)	=	1.2 square yards (sq yd, yd ²)
1 square kilometer (km ²)	=	0.4 square mile (sq mi, mi ²)
10,000 square meters (m ²)	=	1 hectare (ha) = 2.5 acres

MASS - WEIGHT (APPROXIMATE)

1 gram (gm)	=	0.036 ounce (oz)
1 kilogram (kg)	=	2.2 pounds (lb)
1 tonne (t)	=	1,000 kilograms (kg) = 1.1 short tons

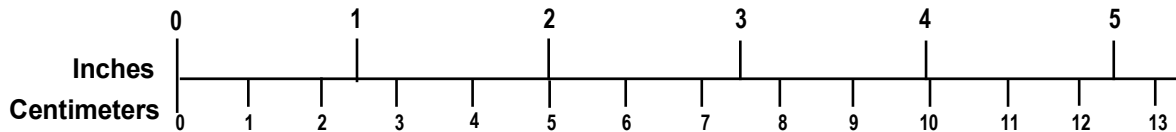
VOLUME (APPROXIMATE)

1 milliliter (ml)	=	0.03 fluid ounce (fl oz)
1 liter (l)	=	2.1 pints (pt)
1 liter (l)	=	1.06 quarts (qt)
1 liter (l)	=	0.26 gallon (gal)
1 cubic meter (m ³)	=	36 cubic feet (cu ft, ft ³)
1 cubic meter (m ³)	=	1.3 cubic yards (cu yd, yd ³)

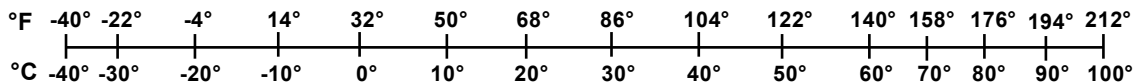
TEMPERATURE (EXACT)

$$[(9/5) y + 32] \text{ } ^\circ\text{C} = x \text{ } ^\circ\text{F}$$

QUICK INCH - CENTIMETER LENGTH CONVERSION



QUICK FAHRENHEIT - CELSIUS TEMPERATURE CONVERSION



For more exact and or other conversion factors, see NIST Miscellaneous Publication 286, Units of Weights and Measures. Price \$2.50 SD Catalog No. C13 10286

Updated 6/17/98

Acknowledgements

The Department of Transportation's John A. Volpe National Transportation Systems Center (Volpe) and the Transportation Technology Center, Inc. (TTCI) authors appreciate the technical advice provided by Jeffrey Gordon of the Federal Railroad Administration's (FRA) Office of Research, Development and Technology. Authors of this report also appreciate the support provided by Melissa Shurland, FRA's technical monitor of this task.

Volpe authors are grateful for the cooperation of the diesel multiple unit manufacturer in providing detailed information on tank construction, design and installation hardware in support of the testing.

Volpe authors gratefully acknowledge the contributions of their colleague Kane Vinson, who aided in computer simulation development during this research program and Dr. A. Benjamin Perlman for his invaluable advice in model development, validation and test design.

TTCI authors acknowledge the contributions of TTCI's test team: Matt DeGeorge, Dwayne Smith, Nash Gonzalez, and Matt Wenger.

Contents

Executive Summary	1
1. Introduction	2
1.1 Background	2
1.2 Objectives	3
1.3 Overall Approach	4
1.4 Scope	4
1.5 Organization of the Report	4
2. Test Requirements and Methods	6
2.1 Test Setup	6
2.2 Test Methods	6
2.3 Test Instrumentation	9
3. Finite Element Model Development	12
3.1 Pre-Test FE Model	12
3.2 Post-Test Model	18
4. Results, Tests, and Analyses	24
4.1 Fuel Tank Impact Results	24
4.2 Comparisons Between FE Models and Test Results	27
5. Conclusion	37
6. References	38
Appendix A – Instrumentation Locations and Technical Specification	39
Appendix B – Fuel Tank Materials	41
Appendix C – Test Data	56
Appendix D – Comparison Between Test Data and Finite Element Analysis Results	63
Abbreviations and Acronyms	65

Illustrations

Figure 1. Flow Diagram of Crashworthiness Research Methodology.....	3
Figure 2. Test Article Mounted on the Impact Wall.....	6
Figure 3. Test Setup	7
Figure 4. Schematic of the DMU Fuel Tank (Bottom View)	8
Figure 5. Impact Cart with Impactor Attached	8
Figure 6. Accelerometer Locations on Ram Car	10
Figure 7. Flowchart of Modeling and Testing Process	12
Figure 8. FE Model Assembly with Annotations	13
Figure 9. FE Model Geometry (Left) and Mesh (Right)	13
Figure 10. Illustration of Weld Modeling.....	14
Figure 11. True Plastic Stress-Strain Behaviors Used in Pre-Test FE Models.....	16
Figure 12. Boundary Conditions on Deformable Cart Model	17
Figure 13. Details of Boundary Conditions and Constraints at Fuel Tank Mounting	18
Figure 14. Fuel Tank End Sheet Sample	19
Figure 15. Fuel Tank Baffle and Side Sheet Samples	19
Figure 16. Engineering Stress-Strain Response from Each Test Sample	20
Figure 17. Comparison of Nominal Stress-Strain Responses from FEA and from Sample Tests of End Sheet Material	21
Figure 18. Comparison of Nominal Stress-Strain Responses from FEA and from Sample Tests of Baffle Material.....	22
Figure 19. Comparison of Nominal Stress-Strain Responses from FEA and from Sample Tests of Side Sheet Material.....	22
Figure 20. Post-Test View of DMU Tank	24
Figure 21. Interior Baffle Deformation.....	25
Figure 22. Deformed Tank Mount.....	25
Figure 23. Deformation – Vertical Cross Section at Impact.....	26
Figure 24. Average Ram Cart Longitudinal Acceleration	27
Figure 25. Average Impact Force	27
Figure 26. Deformed Bottom Sheet from Post-Test Photo (Left), Pre-Test Model with Deformable Impactor (Second from Left) and Pre-Test Model with Rigid Impactor (Second from Right) and Post-Test Model with Deformable Impactor (Right)	28

Figure 27. Side View of Deformed Tank Shape from Post-Test Tank (Left), Pre-Test FE Model with Deformable Impactor at 11.1 mph (Center), and Pre-Test FE Model with Rigid Impactor at 11.5 mph (Right).....	29
Figure 28. Contour Plots (inches) of Longitudinal Deformation from Post-Test Scan (Left), Pre-Test FE Model with Deformable Impactor at 11.1 mph (Center), and Pre-Test FE Model with 11.5 mph Rigid Impactor (Right)	30
Figure 29. Impactor Force Versus Impactor Travel for Pre-Test FEA and Test Data.....	31
Figure 30. Impactor Speed Versus Time for Pre-Test FEA and Test Data	31
Figure 31. Impactor Travel Versus Time for Pre-Test FEA and Test Data.....	32
Figure 32. Impactor Force Versus Impactor Travel for Post-Test FEA and Test Data	33
Figure 33. Impactor Force Versus Time for Post-Test FEA and Test Data	33
Figure 34. Impactor Speed Versus Time for Post-Test FEA and Test Data.....	34
Figure 35. Impactor Travel Versus Time for Post-Test FEA and Test Data	35
Figure 36. Energy Absorbed by Tank Versus Impactor Travel for Test and Post-Test FEA.....	35

Tables

Table 1. Instrumentation Summary.....	9
Table 2. Impact Cart Accelerometers	10
Table 3. Summary of Mesh in Pre-Test FE Models	15
Table 4. Locations of Material Samples	20
Table 5. Summary of Fuel Tank Impact Tests.....	24
Table 6. Comparison of Key Results from Pre-Test FEA, Test, and Post-Test FEA.....	28

Executive Summary

The Federal Railroad Administration's (FRA) Office of Research, Development and Technology has been conducting research into passenger locomotive fuel tank crashworthiness. FRA sponsored ongoing work performed by Transportation Technology Center Inc. (TTCI) at the Transportation Technology Center (TTC) in Pueblo, CO, of a dynamic impact test of a DMU fuel tank, which began on June 28, 2016. The Department of Transportation's John A. Volpe National Transportation System Center (Volpe) supports FRA in evaluating the crashworthiness of fuel tank designs and developing technical research for supporting standard and regulation development. A series of impact tests were conducted and planned for future testing to measure fuel tank deformation under two types of dynamic loading conditions, which are blunt and raking impacts. Test specimens included a set of FRA owned retired passenger locomotive fuel tanks and a set of new diesel multiple unit (DMU) fuel tanks purchased by FRA from a manufacturer currently in passenger rail operation in the US.

TTCI developed specialized hardware and procedures for testing DMU fuel tanks as part of the project. An impact vehicle weighing approximately 14,000 pounds and equipped with a 12-inch by 12-inch impactor head struck the bottom surface of a DMU fuel tank mounted vertically on the impact wall, using the mounting hardware supplied by the manufacturer of the fuel tank. The impact occurred on the bottom of the fuel tank at a location centered on two baffles within the fuel tank. The target impact speed was 11.5 mph, and the measured impact speed was 11.2 mph. The test resulted in a maximum indentation of approximately 8 inches. The bottom of the tank bent away from the wall under impact, resulting in deformation of the mounting hardware as well. Several internal baffles in the impact zone buckled.

Test results were used to validate and refine computer simulations. Volpe developed a finite element (FE) model of the fuel tank and impactor that was used to design the test setup. The targeted impact speed, impact location and behavior of the fuel tank under loading were determined using the FE model. After the test, material samples were cut from several unaffected areas of the DMU fuel tank and subjected to tensile testing. An update was performed to the post-test FE model of the fuel tank with material properties from the tensile test, and due to this update the simulation was rerun. Overall, both the pre- and post-test FE models exhibited very good agreement with the test measurements. The models exhibited similar modes of deformation as the fuel tank exhibited in the test. Both, the models and test resulted in no puncture of the fuel tank under the impact conditions. The correlation of the FE model analysis and the actual test results will allow FRA to use the model to simulate and analyze other impact conditions on this fuel tank, and possible other tanks of similar design.

1. Introduction

The Federal Railroad Administration (FRA) has been conducting fuel tank research to examine strategies for increasing passenger locomotive fuel-tank puncture resistance to mitigate the threat of a post-collision or post-derailment fire. In accidents, fuel tanks can experience dynamic loading, often including a blunt or raking impact from various components of the rolling stock or track bed [1]. Current design practice requires that fuel tanks have minimum properties adequate to sustain a prescribed set of static load conditions. The ongoing research is intended to increase understanding of the structural response of fuel tanks under dynamic loading. By utilizing an approach that has been effective in increasing the structural crashworthiness of passenger railcars, improved strategies can be developed that will address the types of loading conditions observed in collisions or derailment events.

Transportation Technology Center, Inc. (TTCI) conducted three separate impact tests on conventional passenger locomotive fuel tanks at the Transportation Technology Center in Pueblo, CO, which began on June 28, 2016. These preliminary tests on retired locomotive fuel tanks were intended to assist in preparing for impact tests on fuel tanks of a modern design, including developing test requirements and planning instrumentation. The previous tests generally served as a “shakedown” of the test setup to identify any areas for potential improvement to maximize success in future tests including the test described in this report.

Current test plans included a series of impact tests on DMU fuel tanks. Detailed finite element analysis (FEA) models developed by Volpe prior to testing, predicted the behavior of the tanks during impact. Test results provided information to improve the FE models and evaluate the accuracy of pre-test analysis. This report describes the fourth test of the blunt impact test series.

1.1 Background

Passenger fuel tank crashworthiness research is conducted as part of FRA’s Rolling Stock Equipment Research program. Current research investigates fuel tank crashworthiness during dynamic impacts. DMU fuel tanks are smaller than conventional passenger locomotive fuel tanks, but are currently required to meet the same standards and regulations.

The Code of Federal Regulations (CFR) requires that Tier I (operations at speeds of 125 mph and less) passenger locomotive fuel tanks have minimum structural properties adequate to sustain a prescribed set of static load conditions [2] [3]. Currently, these requirements apply to all equipment defined as a locomotive, which includes alternative equipment, such as DMUs. As such, FRA’s Office of Research, Development and Technology is conducting research into passenger locomotive fuel tank crashworthiness to determine how well existing regulations for conventional fuel tanks apply to alternative fuel tanks. Current research is intended to increase understanding of the impact response of fuel tanks under dynamic impact conditions and propose strategies for DMUs to meet a minimum level of safety. The research program is designed to first assess conventional passenger locomotive fuel tanks and then assess alternatively designed passenger equipment fuel tanks.

The research program follows the methodology shown in Figure 1, which begins with developing a baseline measure of existing design performance for a given scenario and extends to developing improvements for enhancing safety performance for that scenario.

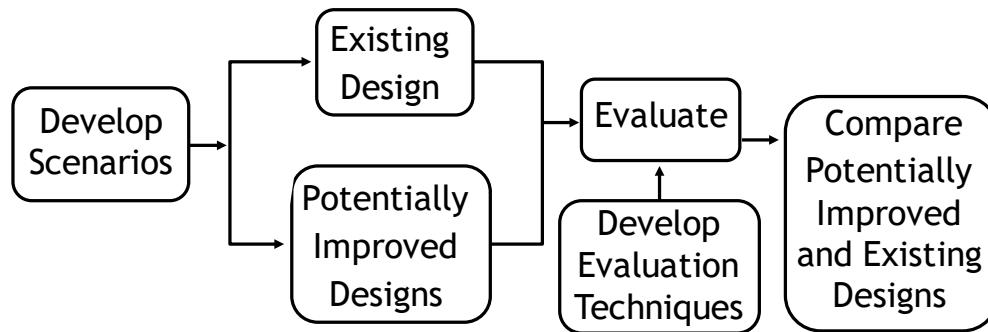


Figure 1. Flow Diagram of Crashworthiness Research Methodology

To develop scenarios for the fuel tank research, FRA conducted a survey of accidents and derailments in the United States over the last two decades [1]. The survey was conducted using the FRA accident database and includes freight and passenger train fuel tanks that reported a fuel tank breach during a collision or derailment. Two key findings should be noted from the results of this survey. First, a fuel tank breach during a train collision or derailment may result in a fire, which presents additional threats to the survivability of passengers and crew as they egress from the collision wreckage. With DMU passenger operations, the risk profile is higher with the presence of more people on board the vehicle and their proximity to the ejected fuel. The second key finding is that each fuel tank impact scenario can be categorized by its resultant loading type, of which there are two general loading conditions leading to punctures: blunt impacts and raking impacts.

A series of full-scale tests is underway to test fuel tanks under the stated impact types. A test setup for a blunt impact was designed and tested on three retired F40 locomotive fuel tanks [4] [5] [6]. The first two blunt impact tests were used to develop a repeatable test setup for conducting a blunt impact of fuel tanks and the third test produced initial information on the performance of conventional fuel tanks under a dynamic impact.

This test report describes the preparation, modeling, and results from the latest fuel tank test in this testing series, a blunt impact of a DMU fuel tank.

1.2 Objectives

The key objective of the impact testing of fuel tanks is to examine the gross response of the fuel tanks to a given impact type. The blunt impact test was designed to characterize each test specimen's deformation behavior when impacted on the bottom sheet. The overall approach to characterizing the deformation behavior includes:

1. Develop an analytical model of the fuel tank specimen based upon known design details.
 - a. Use the analytical model to plan for tests.
 - b. Estimate possible fuel tank behavior under test impact conditions.
2. Apply a blunt, dynamic load to the bottom surface of a fuel tank specimen.
 - a. Measure the force-deflection behavior of the tank with specified instrumentation.
 - b. Record mode of deformation with high speed and conventional video cameras.

- c. Record permanent deformation by surface light detection and ranging (LIDAR) scans.
3. Conduct post-test examination of the tank.
 - a. Characterize structural deformation of tank exterior and interior.
 - b. Cut material samples from various areas of tank and perform tensile testing to characterize mechanical properties.
4. Update the model with actual test speed and tank material properties.
5. Evaluate the accuracy of the model.

The outcome of this process can be used to make a comparison between fuel tanks of different designs, with analysis techniques being used to provide additional information on the fuel tank behavior. Modeling can also be used to simulate additional impact conditions beyond what was tested, providing additional points of comparison between different designs. The results of the first two tests of passenger locomotive fuel tanks gave preliminary insight into the deformation patterns of conventional fuel tanks and helped to demonstrate the functionality of the dynamic blunt impact test setup at TTC. The third (conventional locomotive) and fourth (DMU) tests, both conducted at approximately 11 mph, provided data that allowed a comparison of the performance of a conventional passenger locomotive fuel tank with that of a DMU fuel tank.

1.3 Overall Approach

This testing effort used FE modeling in conjunction with full-scale testing to better understand the behaviors of a DMU fuel tank under similar blunt impact conditions to those used to test the retired passenger locomotive fuel tanks. Prior to the test, engineering drawings and computer-aided design (CAD) geometry were used to generate a detailed FE mesh of the fuel tank. Material responses, including plastic stress-strain responses, were estimated for the materials making up the fuel tank. The pre-test FE model was used to plan for instrumentation range and placement, as well as to estimate the desired test speed. The test was conducted according to the test plan. The results of the test were used to compare the response of the DMU tank with the response of the retired F40-type fuel tanks under similar impact conditions, and to verify the results of the FE model. After the test, material samples were cut from the fuel tank and subjected to tensile testing. These results were used to update the FE model, which was then run at the measured test speed.

1.4 Scope

This report describes the test preparations, instrumentation, and the data collected from the test. It also includes discussion of the development of the pre-test FE model, and modifications to the materials of the model after the test to reflect the actual material used in construction of the tank. Additionally, future test plans are discussed in this report to provide context.

1.5 Organization of the Report

This report is organized into six sections, five of which are outlined. Section 2 describes the test setup for the blunt impact test conducted on four fuel tank specimens to date and the specific details of installing the DMU tank. Section 3 provides an overview of the computer simulation used to model the responses of the fuel tanks to the impacts. Section 4 presents the results from

the tests and the corresponding computer simulations, and compares these results to one another. Section 5 contains concluding remarks and discussion about the testing and analysis program. Four appendices provide additional details on the instrumentation location and test requirements, fuel tank material properties, test data, and comparison of the pre-test and post-test model results with the measurements made during the test.

2. Test Requirements and Methods

The following sections will discuss the test requirements and methods for the DMU fuel tank impact test.

2.1 Test Setup

DMU fuel tank impact test was conducted on the impact wall at the TTC. TTCI designed mounting brackets to support the fuel tank on the impact barrier face. The brackets were aligned with the existing connections on the tank and they created a small gap between the impact wall and the tank's top surface. Once mounted, the impact point was aligned with the impactor on the ram cart. The mounting method created a support condition similar to how the fuel tank is installed to the underframe of the DMU. Mounting hardware used to mount the fuel tank to the impact wall was typical for installation of the fuel tank on the DMU, and was provided by the DMU manufacturer. They include a 20mm [0.787 inch] diameter bolt, rubber bushing, and set of washers for each mounting location. Figure 2 shows mounting of the test article on the impact wall and a detail photo of the installation hardware.

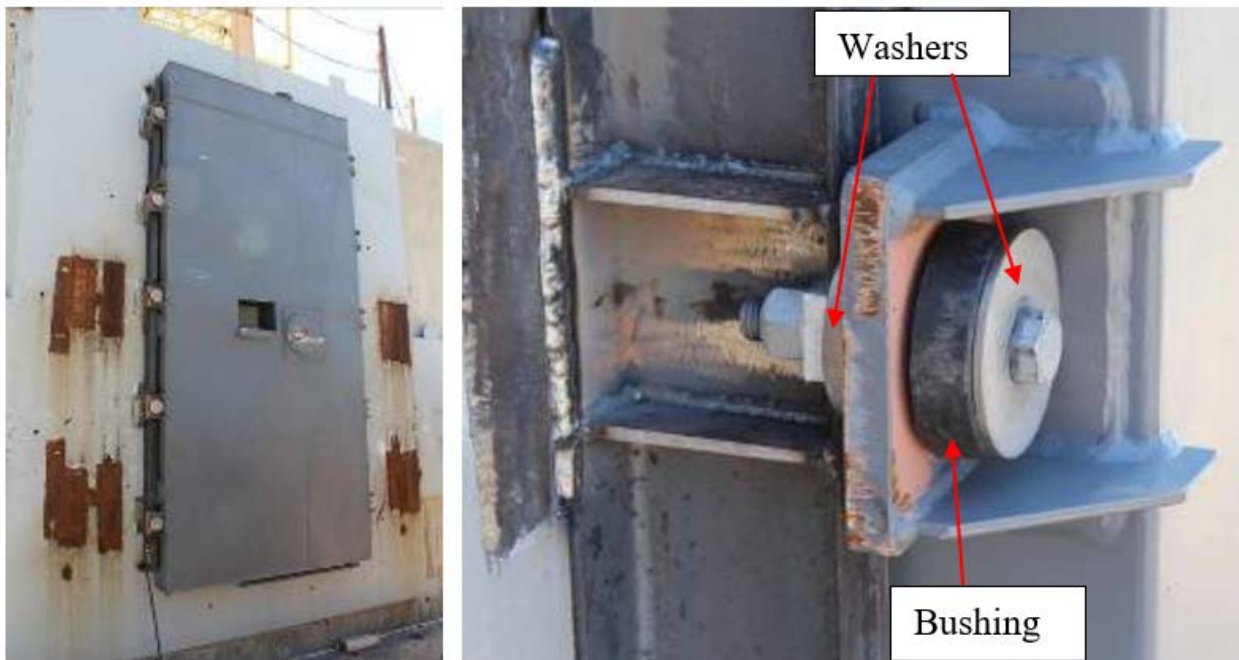


Figure 2. Test Article Mounted on the Impact Wall

2.2 Test Methods

The test requirements contained in this document were developed cooperatively among FRA, Volpe, and TTCI.

The fuel tank was supported directly on the impact wall as described in Section 2.1. The test article was positioned to align with a 12-inch by 12-inch impactor for the center impact. Figure 3 illustrates the test setup mounted to the impact wall. More photos before and after the tests are provided in Appendix A.



Figure 3. Test Setup

This fuel tank alignment provided for center impact at the tank's bottom side. The impact location for this DMU fuel tank was on an intersection of lateral and longitudinal baffles inside the tank. Figure 4 shows the internal layout of the fuel tank baffles and the impact location (shown in red). Figure 5 shows the 12-inch by 12-inch square impactor attached to a moving ram cart. The total weight of the ram cart including impactor was 14,075 pounds. The target impact speeds were specified based on preliminary analysis, to maximize the amount of deformation in the tank without allowing the ram to solidly compress the baffle or puncture the fuel tank. The data collected during the test included accelerations, impact speed, and both high speed and real-time video recordings.

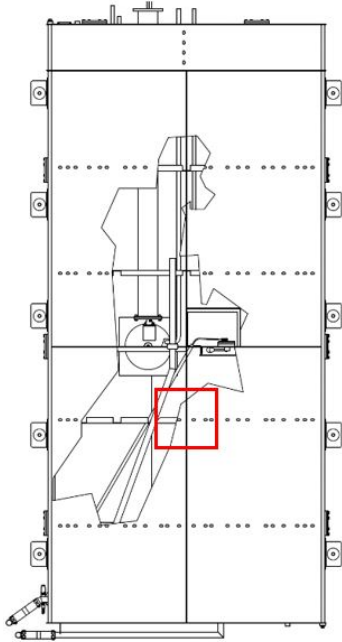


Figure 4. Schematic of the DMU Fuel Tank (Bottom View)



Figure 5. Impact Cart with Impactor Attached

2.3 Test Instrumentation

Test instrumentation used in the DMU fuel tank blunt impact test is discussed below.

2.3.1 Definition of Coordinate Axes

All local acceleration and displacement coordinate systems are defined relative to the impact vehicle. Positive x, y, and z directions are forward, left, and up relative to the lead end of the impact vehicle.

2.3.2 Impact Cart Accelerometers and Speed Sensors

Three tri-axial accelerometers were mounted at the two ends and close to the center along the ram cart center line. Three tri-axial accelerometers were also mounted on the left and right sides of the middle of the ram cart (Figure 6).

TTCI installed redundant speed sensors on each side of the cart to accurately measure the impact speed within 2 feet of the impact point. The speed traps are reflector-based sensors. They use ground-based reflectors separated by a known distance and vehicle-based light sensors that trigger as the ram cart passes over the reflectors. The last reflector was within 1 inch of the impact point. The time interval between passing the reflectors was recorded. Speed was then calculated from distance and time. TTCI also used a handheld radar gun to take supplemental speed measurements. Table 1 shows the summary of instrumentation, Table 2 shows the accelerometer details and Figure 6 illustrates the sensor locations.

Table 1. Instrumentation Summary

Type of Instrumentation	Channel Count
Accelerometers	12
Speed Sensors	2
Total Data Channels	14

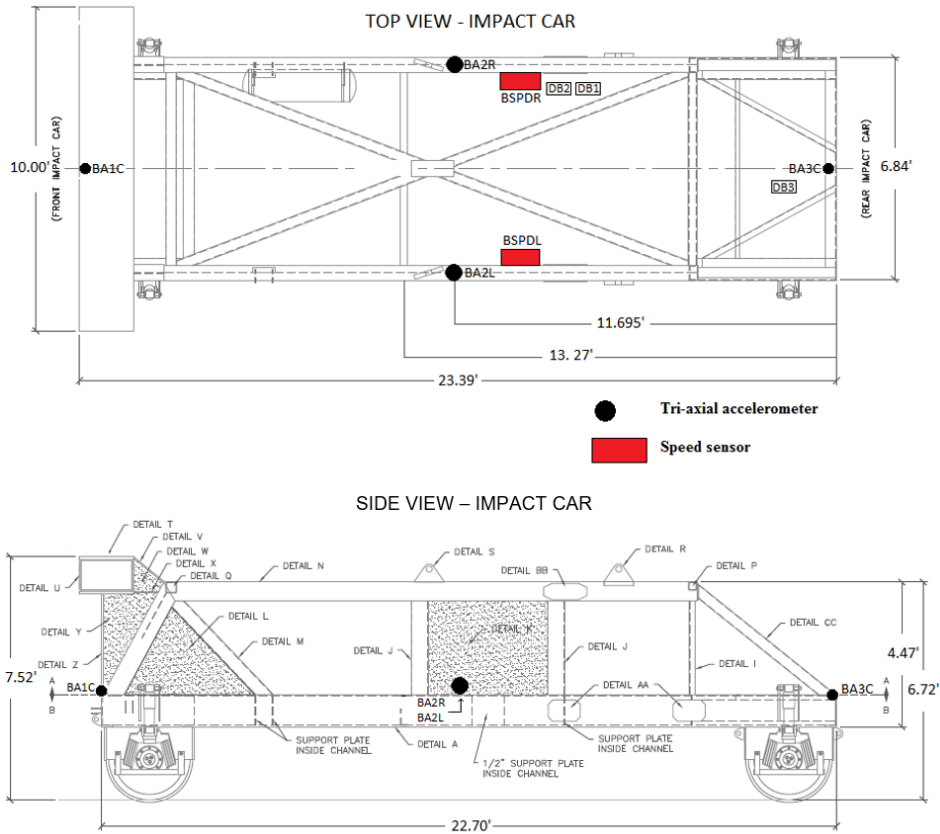


Figure 6. Accelerometer Locations on Ram Car

Table 2. Impact Cart Accelerometers

Channel Name	Sensor Description	Range
BA1CX	Leading end, Centerline, X Accel	100g
BA1CY	Leading end, Centerline, Y Accel	100g
BA1CZ	Leading, Centerline, Z Accel	100g
BA2LX	Middle, Left Side X Accel	100g
BA2LY	Middle, Left Side Y Accel	100g
BA2LZ	Middle, Left Side Z Accel	100g
BA2RX	Middle, Right Side X Accel	100g
BA2RY	Middle, Right Side Y Accel	100g
BA2RZ	Middle, Right Side Z Accel	100g
BA3CX	Trailing end, Centerline, X Accel	200g
BA3CY	Trailing end, Centerline, Y Accel	200g
BA3CZ	Trailing end, Centerline, Z Accel	200g

2.3.3 Real Time and High-Speed Photography

Three high speed and three real time high definition video cameras documented the impact event. Appendix A shows a schematic of the locations of the cameras and the positions of the targets that were installed on the fuel tank and on the impact cart.

2.3.4 Data Acquisition

Two 8-channel battery-powered onboard data acquisition systems recorded data from instrumentation mounted on the ram cart. These systems provided excitation to the instrumentation, analog anti-aliasing filtering of the signals, analog-to-digital conversion, and recording of each data stream.

The data acquisition systems were GMH Engineering Data BRICK Model II units. Data acquisition complied with the appropriate sections of SAE J211 [7]. Data from each channel was anti-alias filtered at 1,735 Hz then sampled and recorded at 12,800 Hz. Data recorded on the Data BRICKs was synchronized to time zero at initial impact. The zero-time reference was triggered from closure of tape switches on the front of the impactor. The Data BRICKs can withstand shock loading up to at least 100 g. Onboard battery power was provided by GMH Engineering 1.7 A-hr 14.4-Volt NiCad battery packs. Tape Switches, Inc., model 1201-131-A tape switches provided the timing of the initial contact event.

Software in the Data BRICKs was used to determine zero levels and calibration factors rather than relying on set gains and expecting no zero-drift. The Data BRICKs recorded 1 second of data before initial impact and 4 seconds of data after initial impact.

2.3.5 Laser Scanning

The impact surface of the fuel tank was scanned both before and after testing. These scans allow for a direct comparison with pre- and post-test FE models by generating a digital, 3D representation of both the undeformed tank and the residual post-test deformation of the tank. These scans are done using a Trimble Total Station. The Trimble Total Station takes laser based distance measurements at discrete 1 degree intervals. This results in a point cloud with variable density. For this test, adjacent points in the point cloud were never more than 5.5 inches apart.

3. Finite Element Model Development

This program used a combination of FE modeling and impact testing to study the impact response of several fuel tank designs. Phase I of this research program included testing of three retired F-40 style passenger locomotive fuel tanks [1] [4] [5] [6]. Phase II featured a blunt impact test of a DMU fuel tank from a DMU design currently in operation within the United States. While much of the Phase I modeling effort was dedicated to measuring the fuel tank geometry, the DMU fuel tank model was based upon drawings and a CAD model provided by the DMU fuel tank manufacturer. The geometry-creation stage of DMU fuel tank modeling was focused on simplifying the highly detailed CAD model to form a reasonable FE mesh, and defining connections between discrete parts where such parts are attached in the actual tank.

The information provided by the DMU manufacturer included the specifications of the materials of construction used in the tank, but it did not include actual tensile sample results. Although this material data is a key input to the FE model, the decision was made not to compromise the fuel tank by cutting material samples from it before the test. Rather, information on material specification was taken from publicly available data generated by other researchers where tensile testing of the same material has been performed to develop pre-test material models. After the testing completed, material samples were cut from undeformed regions of the DMU tank to obtain the actual tensile behavior of the materials, and the post-test models were updated. The pre-test model and the test results were found to be in very good agreement with one another. There was no need to adjust any of the boundary conditions in the pre-test model, except to run the model at the measured impact speed of 11.2 mph. The pre-test material behavior was replaced by the actual material behavior after the test, which did not have a substantial effect on the good agreement between the model and the test data. The overall modeling and testing approach used in Phase II is represented schematically in Figure 7.

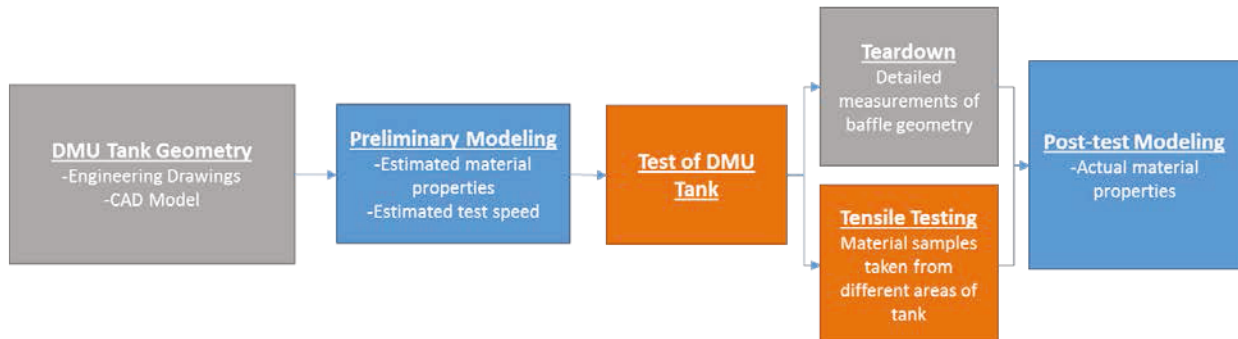


Figure 7. Flowchart of Modeling and Testing Process

3.1 Pre-Test FE Model

The commercial FE solver Abaqus/Explicit 6.14-2 was used to perform the simulations of both the pre- and post-test models [8]. The development of the geometry for the pre-test FE model is described in the following sections.

3.1.1 Geometry

An overview of the pre-test FE model is shown in Figure 8. Details of the mounting assembly are shown in the top left detail.

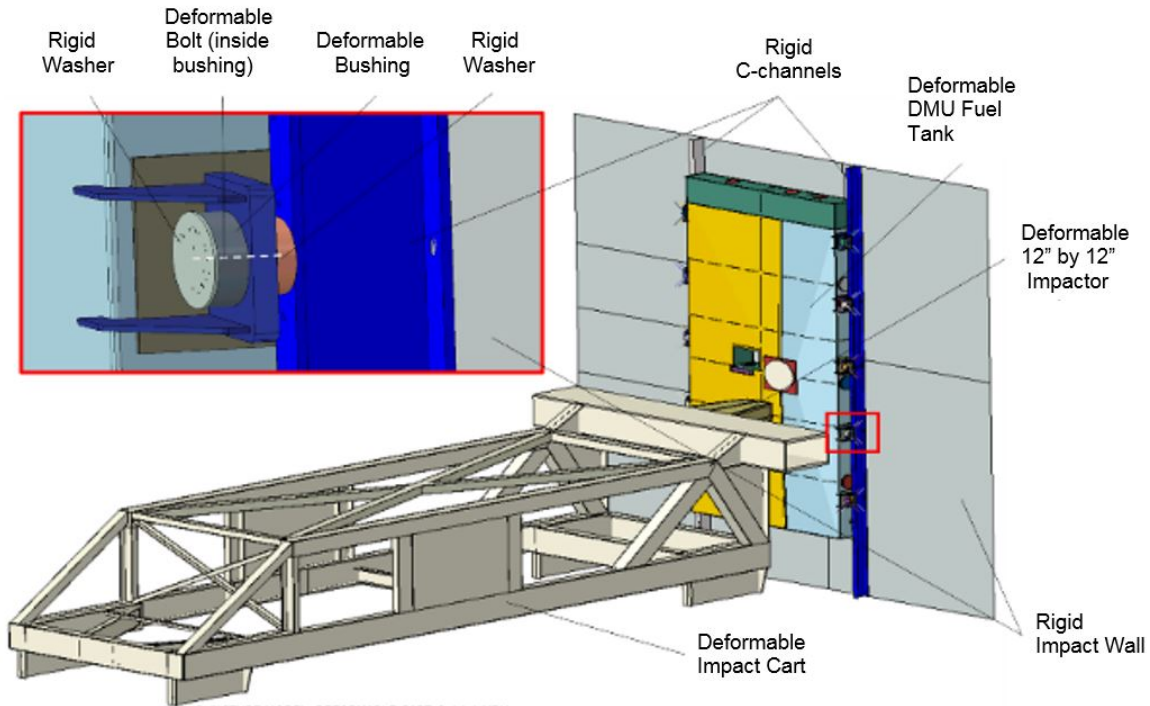


Figure 8. FE Model Assembly with Annotations

Detailed information on the geometry of the DMU fuel tank was provided by the manufacturer as part of the purchase of the tank. The information included engineering drawings as well as a CAD file that was used as a starting point for the tank geometry in the FE model. Because the CAD geometry was highly detailed, it was necessary to simplify the geometry to produce a reasonable FE mesh. Additionally, the CAD model represented the true 3D geometry of the tank as a solid, with the thicknesses of various components modeled explicitly. Because the FE model was intended to be made of shell elements, it was necessary to convert the solid CAD geometry into faces upon which shell elements could be meshed. Figure 9 shows the shell geometry in the FE model on the left, alongside the resulting shell mesh on the right.

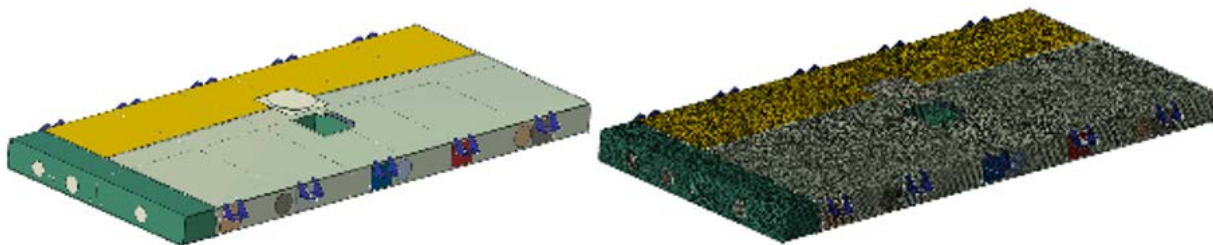


Figure 9. FE Model Geometry (Left) and Mesh (Right)

The CAD model defined each component as a separate part within an assembly, but did not define any connections between the parts. Thus, as a part of the model creation process it was necessary to define behaviors for how the components would interact with one another. While

merging individual parts and using shared nodes to mesh would have reduced the number of nodes and elements in the model. The tied constraint approach would allow the connections to be studied in more detail should weld failure have been observed during the test. General contact was defined for the entire model, enabling the complex contact that results from a baffle folding up onto itself to be captured. Additionally, tied constraints were used to simulate attachments between parts that were welded to one another in the physical tank. The tied constraints between parts constrain all six degrees-of-freedom (DOF) (three translational and three rotational) between defined nodes, and cannot fail. In this way, the constraints represent a perfectly welded connection between parts. An example of this constraint is shown in Figure 10, where a tied constraint is used to simulate a slot weld between the top sheet of the fuel tank and the top of an internal baffle. In this image, individual parts have different colors assigned to one another, and the tied constraint appears as a series of lines between the corresponding nodes of the two parts.

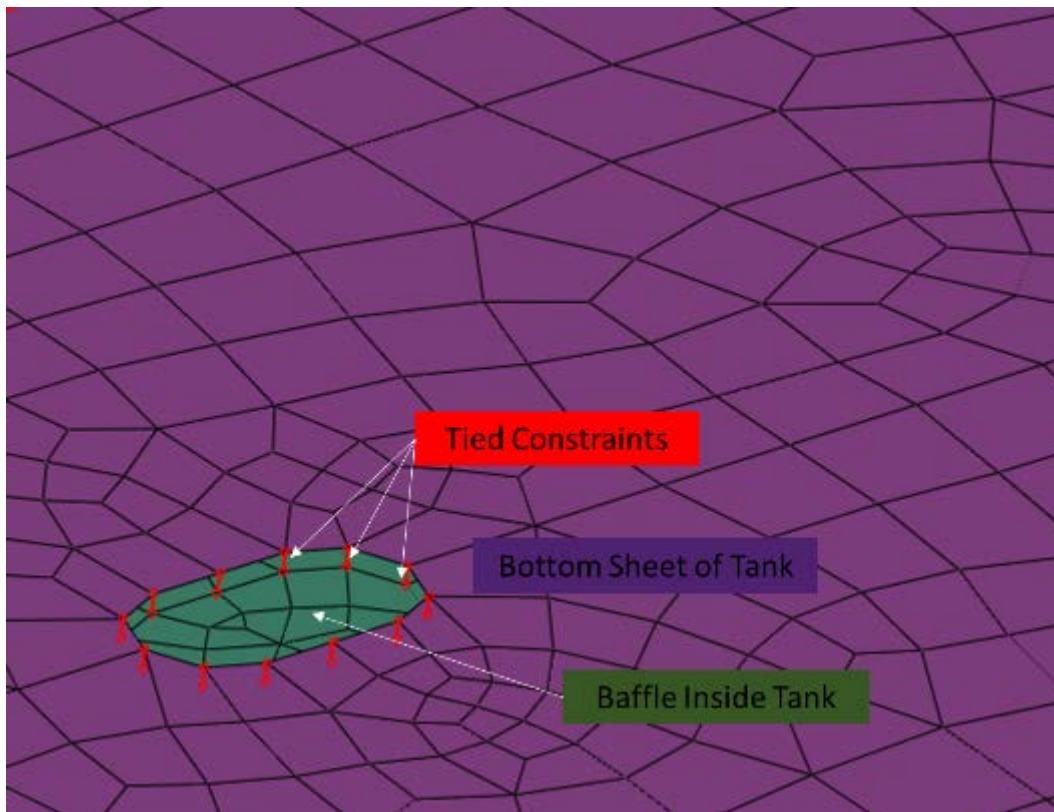


Figure 10. Illustration of Weld Modeling

While the DMU fuel tank itself was meshed using deformable shell elements, other structures within the assembly were meshed using other modeling techniques. The mesh techniques used in the pre-test FE models are summarized in Table 3.

Table 3. Summary of Mesh in Pre-Test FE Models

Part Name	Element Type	Number of Elements
Deformable Cart	Reduced Integration Quadrilateral Shell (S4R)	66,141
Deformable Cart	Reduced Integration Triangular Shell (S3R)	126
Deformable 12 x 12 Impactor	Reduced Integration Quadrilateral Shell (S4R)	23,718
Deformable Tank	Fully integrated Quadrilateral Shell (S4)	7,087
Deformable Tank	Reduced Integration Quadrilateral Shell (S4R)	171,935
Deformable Tank	Reduced Integration Triangular Shell (S3R)	2,987
Deformable Rubber Bushing	Reduced Integration Hexahedral Continuum (C3D8R)	8,400
Deformable Bolt	Quadratic Beam (B32)	10
Rigid Wall	Rigid Quadrilateral (R3D4)	400
Rigid Wall	Rigid Body Reference Node (RNODE3D)	11
Rigid Washer (thin)	Rigid Quadrilateral (R3D4)	2,213
Rigid Washer (thin)	Rigid Triangle (R3D3)	38
Rigid Washer (thin)	Mass Element	1
Rigid Washer (thin)	RNODE3D	1
Rigid Washer (thick)	Rigid Quadrilateral (R3D4)	1,759
Rigid Washer (thick)	Rigid Triangle (R3D3)	36
Rigid Washer (thick)	Mass Element	1
Rigid Washer (thick)	Rigid Body Reference Node (RNODE3D)	1
Rigid C-channel	Rigid Triangle (R3D3)	198
Rigid C-channel	Rigid Quadrilateral (R3D4)	22,413
Rigid C-channel	Rigid Body Reference Node (RNODE3D)	5
Rigid 12 x 12 Impactor	Rigid Triangle (R3D3)	4
Rigid 12 x 12 Impactor	Rigid Quadrilateral (R3D4)	7,268
Rigid 12 x 12 Impactor	Mass Element	1
Rigid 12 x 12 Impactor	Rigid Body Reference Node (RNODE3D)	4

3.1.2 Materials

While the tank drawings included information on the material specifications of the different parts used to make the tank, no test data from the actual materials of construction were available. Because elastic-plastic material behaviors needed to be defined in the pre-test FE model, this behavior had to be approximated based on available information, and would be updated with actual test data after the impact test. The tank featured two different steel alloys, referred to as S235 and S355 in this report. For each material, a value of 200 GPa (2.9×10^7 psi) was used for Young's modulus. Because excising tensile test samples from the tank prior to the impact test could potentially compromise the integrity of the tank as a test article, other sources of plastic stress-strain data were sought for use in the pre-test FE model. The input data for the S235 and S355 materials were adapted from stress-strain data published by a steel manufacturer for similar alloys of steel [9]. A piecewise material model was defined for both materials as a function of true stress and true plastic strain. The material responses used in the pre-test FE model are shown in Figure 11. A description of the process of creating the pre-test material responses, and tabular values for stress and strain used as inputs for the pre-test model are provided in Appendix B.

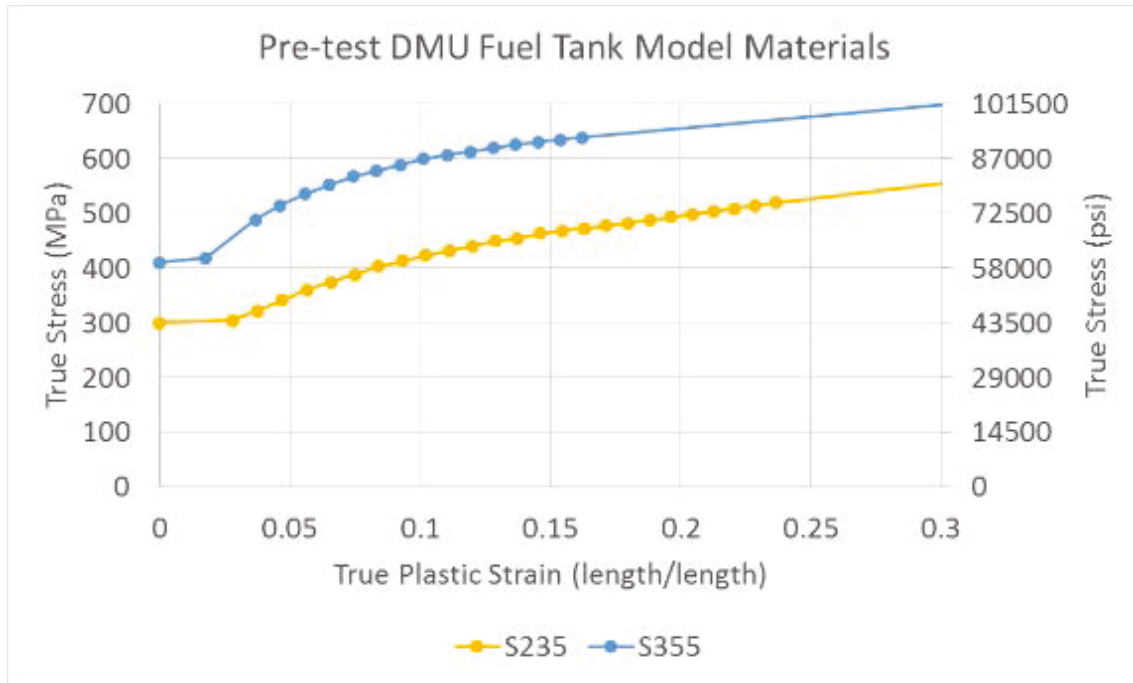


Figure 11. True Plastic Stress-Strain Behaviors Used in Pre-Test FE Models

3.1.3 Boundary and Initial Conditions

A series of boundary and initial conditions were applied to the parts in the model to provide a reasonable representation of the constraints provided by the test setup. Due to the unique geometry of the DMU fuel tank, no symmetry conditions were used in any of the FE models.

Impact Wall

The rigid impact wall was constrained against motion in all six DOF.

Impactor

The impactor was represented both as a rigid body having the mass of the cart at the impact face, and as a deformable impactor and cart. The rigid impactor model was used to generate preliminary data that allowed the test setup to be refined, which in turn provided more precise speed and impact location inputs for the deformable cart model. For the model run using the rigid impact head, the impactor was only allowed to translate longitudinally (i.e., toward or away from the impact wall), and was constrained against motion in all other DOF. For the deformable impact cart, the locations where the axles would attach to the physical cart were constrained against vertical motion. The locations of the vertical boundary conditions on the deformable cart are indicated in Figure 12.

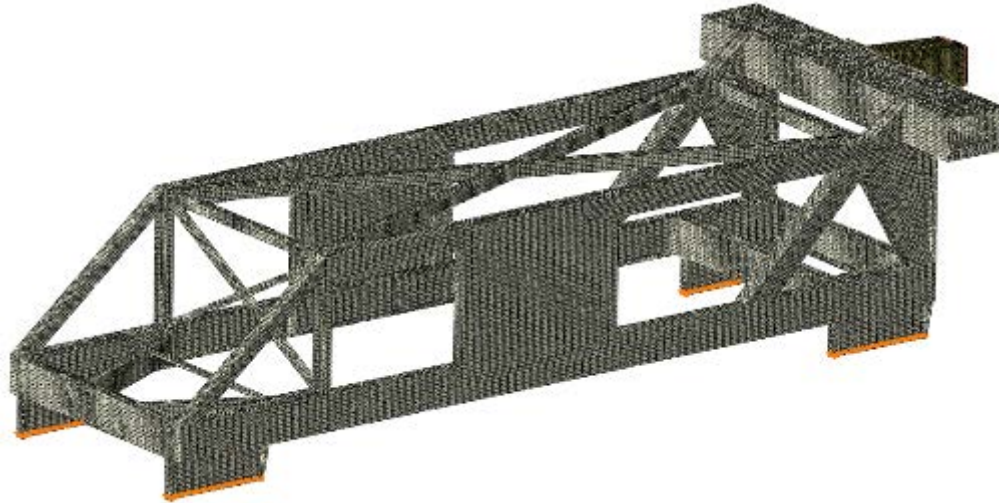


Figure 12. Boundary Conditions on Deformable Cart Model

For all impact models, the impactors were given an initial velocity and allowed to slow down as their kinetic energy was transferred into the tank. For the rigid impactor, the rigid body reference node was the only location for which an initial longitudinal velocity was defined. For the deformable cart models, all nodes within the cart-impactor assembly were given an initial longitudinal velocity.

Tank-to-Wall Mounting

The mounting arrangement used in the model was intended to emulate the actual mounting as closely as possible. The tank itself did not have any boundary conditions placed on it. Rather, the tank was constrained through contact with the mounting hardware, which itself was constrained using boundary conditions. Figure 13 shows a translucent view of the typical mounting arrangement used in all FE models. Note that in this figure the DMU tank has been hidden to clarify the mounting arrangement. Each deformable bracket on the tank does not have any boundary conditions or constraints on it, but is in contact with a rubber bushing. The bushing had a deformable bolt running through it, and featured a thin rigid washer on one end of it and a thick rigid washer on the other. The deformable bolt featured a tied constraint on each end, with a constraint tying the end of the bolt to the thick rigid washer, and a constraint tying the other end of the bolt to the thin rigid washer. The thick rigid washer featured a boundary condition that prevented motion in all DOF. Thus, the corresponding end of the deformable bolt was also constrained against motion in all DOF through its tie to the thick rigid washer. Additionally, the rigid channels between the bolts and the impact wall were also constrained in all six DOF.

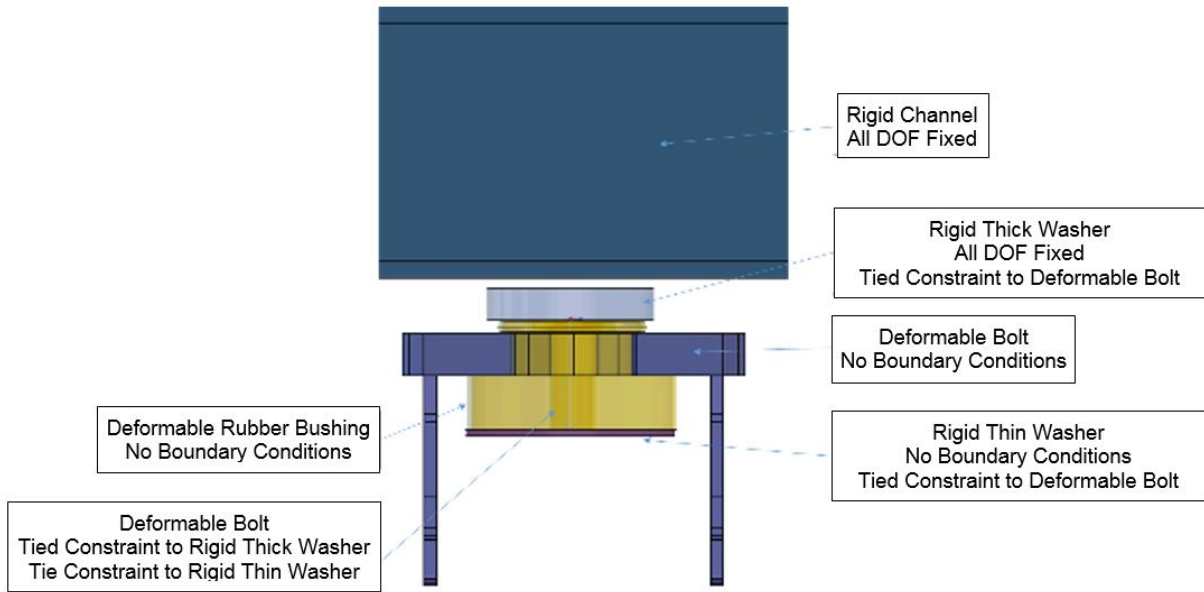


Figure 13. Details of Boundary Conditions and Constraints at Fuel Tank Mounting

3.2 Post-Test Model

The proceeding sections will discuss the post-test modeling activities of the DMU blunt impact test.

3.2.1 Geometry

The post-test model used identical geometry as the pre-test model. As the pre-test model geometry was derived from engineering drawings and an electronic CAD model of the tank provided by the manufacturer, there was no need to update the post-test model geometry based on any unexpected geometric discrepancies discovered during the testing or the post-test teardown.

3.2.2 Materials

After the test, material samples were cut from three areas of the tested DMU tank: the front sheet, the side sheet, and one of the internal baffles, as shown in Figure 14 and Figure 15. The material samples were subjected to tensile testing to determine their actual stress-strain and elongation behaviors. These test results were used to generate new material behaviors, which were updated in the post-test FE models.

The initial FEA was based on material properties from the manufacturer specification, due to the fact that this tank was new and never used in service. After the impact tests, a total of nine samples were cut from the test article and sent for analysis. Locations of each sample are listed in Table 4. The yield strength of the fuel tank steel was found to be lower than the yield strength that was used for the initial FEA. Results from material tests and a more thorough description of the process of developing the material responses appear in Appendix B.



Figure 14. Fuel Tank End Sheet Sample

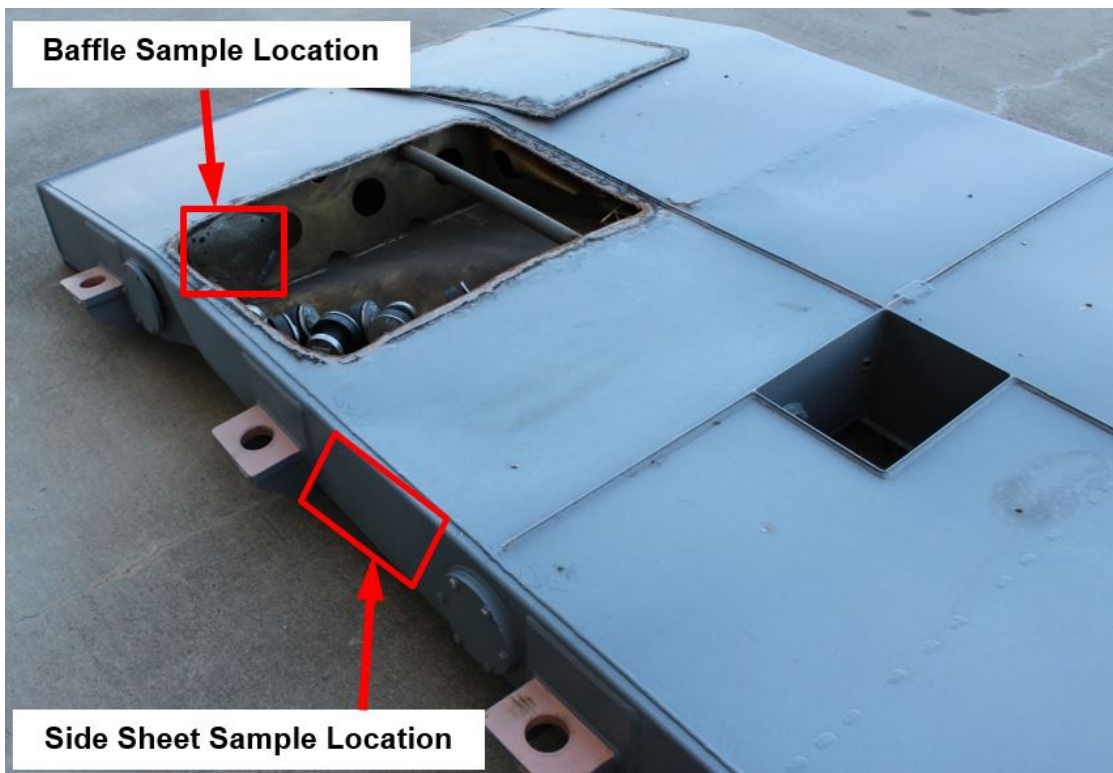


Figure 15. Fuel Tank Baffle and Side Sheet Samples

Table 4. Locations of Material Samples

Location	ID	Ultimate Tensile Strength (ksi)	Ultimate Tensile Strength (MPa)	Yield Strength (ksi)	Yield Strength (MPa)	Elongation at Failure %
End Sheet	S1	66.5	458.5	46.6	321.3	34
End Sheet	S2	66.7	459.9	46.0	317.2	31
End Sheet	S3	66.9	461.3	46.8	322.7	33
Baffle	B1	74.8	515.7	51.5	355.1	32
Baffle	B2	73.9	509.5	51.0	351.6	34
Baffle	B3	73.7	508.1	50.8	350.3	33
Side Sheet	SD1	68.6	473	50.7	349.6	29
Side Sheet	SD2	69.2	477.1	50.2	346.1	31
Side Sheet	SD3	69.6	479.9	51.7	356.5	32

The plastic portion of the nominal stress-strain responses from these nine samples are plotted in Figure 16.

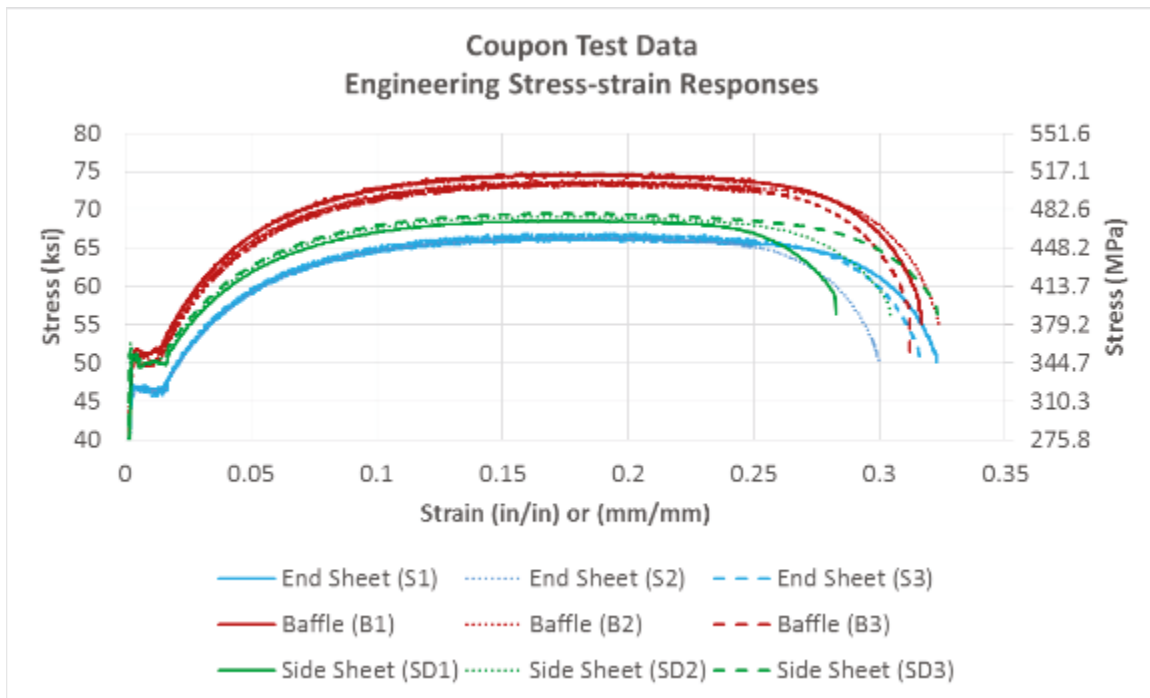


Figure 16. Engineering Stress-Strain Response from Each Test Sample

Using these test data, three post-test material responses were developed for use in the post-test FE models. Each material characterization required the definition of a series of true stress, true plastic strain points to form a piecewise linear curve. Additionally, damage initiation and progression behaviors had to be defined to allow the materials to simulate puncture. Using an iterative approach, the combination of plastic stress-strain response, damage initiation envelope, and damage progression were used to define materials that simulate the tensile response of the actual materials. The engineering (nominal) stress-strain responses calculated from the test results for a given material were then compared with the engineering stress-strain response calculated from the FE simulation for that material sample. The material input data was adjusted until reasonable agreement was obtained between engineering stress-strain responses, including

strain-to-failure. The engineering stress-strain responses are shown in Figure 17 for the end sheet, Figure 18 for the baffles, and Figure 19 for the side sheet.

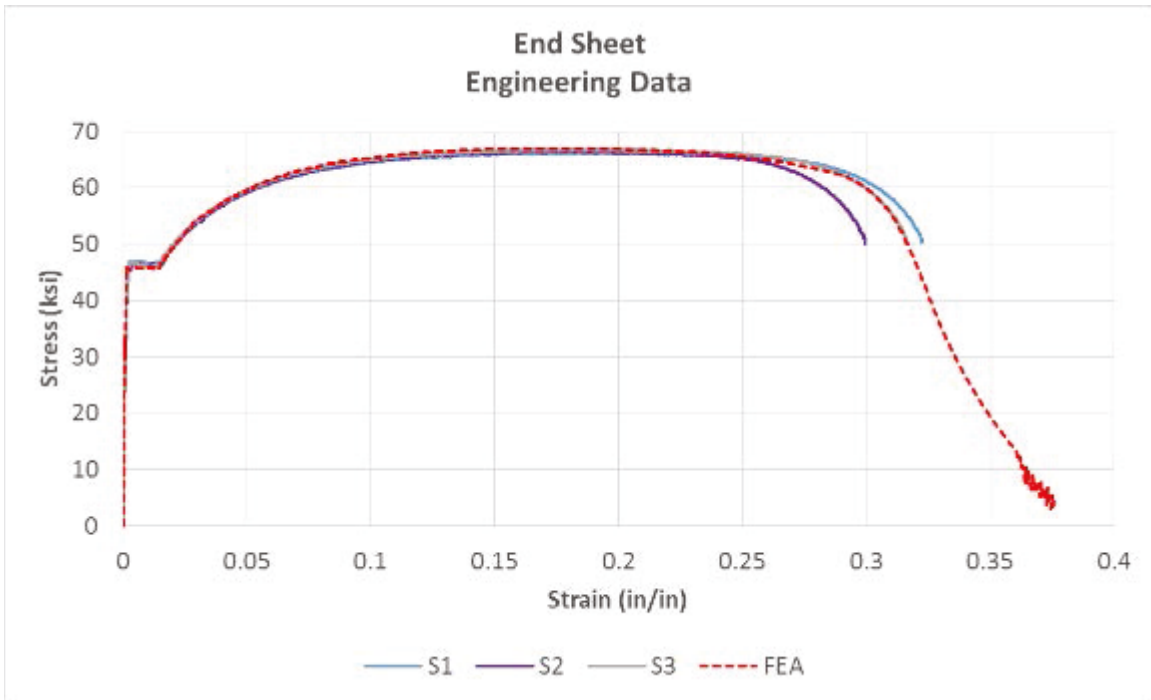


Figure 17. Comparison of Nominal Stress-Strain Responses from FEA and from Sample Tests of End Sheet Material

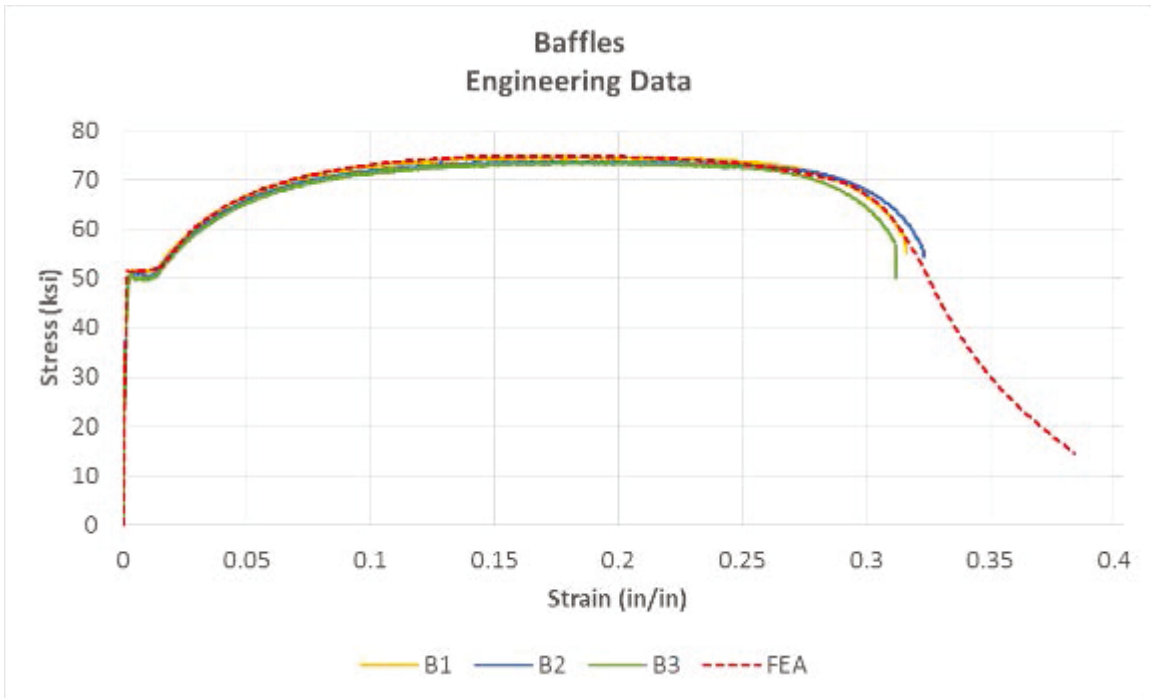


Figure 18. Comparison of Nominal Stress-Strain Responses from FEA and from Sample Tests of Baffle Material

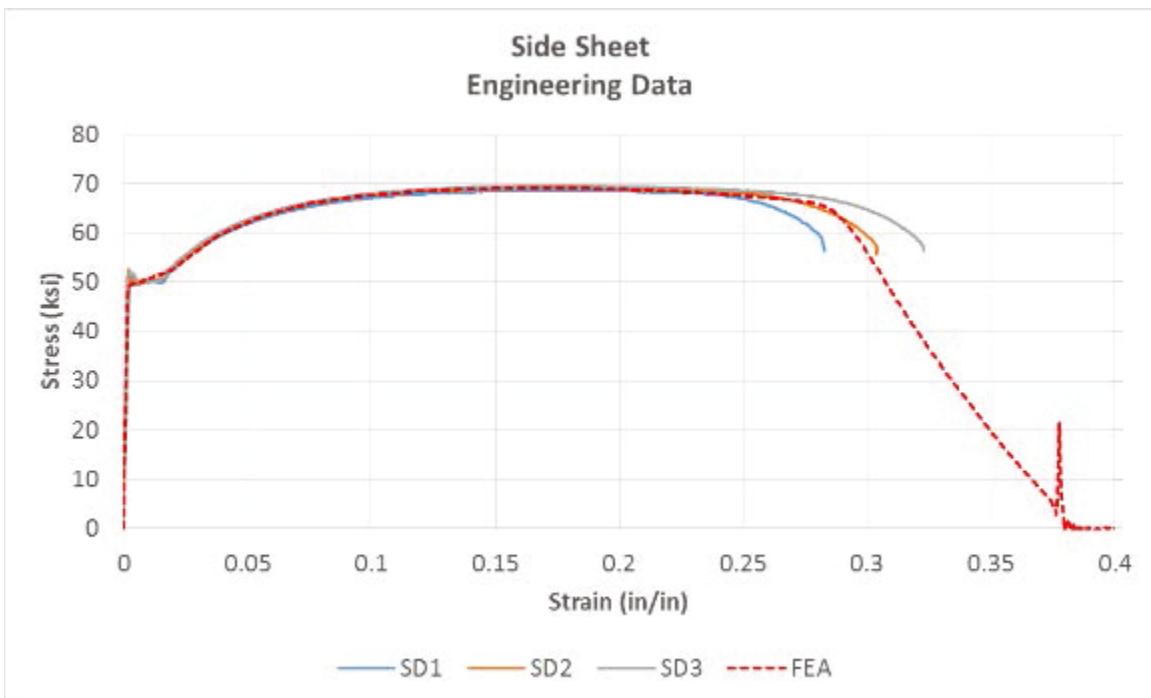


Figure 19. Comparison of Nominal Stress-Strain Responses from FEA and from Sample Tests of Side Sheet Material

3.2.3 *Boundary and Initial Conditions*

The post-test model used identical boundary conditions as the pre-test model. The initial speed of the impact cart was updated in the post-test model to match the impact speed measured in the test.

4. Results, Tests, and Analyses

The results of the impact test are summarized in Table 5. In this section, the post-test FE models are discussed unless otherwise specified. The complete set of test and analysis results can be found in Appendix C and Appendix D.

Table 5. Summary of Fuel Tank Impact Tests

Test Date	Target Speed	Impact Speed	Impact Force	Impact Energy	Result
June 28, 2016	11.5 mph	11.2 mph	~155,000 lbf	~58,000 foot-lbf	~6.3 inch residual dent No puncture

4.1 Fuel Tank Impact Results

The target speed for this impact was 11.5 mph. The actual measured impact speed from the speed traps was 11.2 mph. The impact dented, but did not puncture the bottom sheet of the tank. The maximum permanent deformation was approximately 6.3 inches. Figure 20 shows the final indentation of the tank. The two baffles that intersect at the impact location buckled during impact.



Figure 20. Post-Test View of DMU Tank

Figure 21 shows the deformation of the tank baffles near the impact location after removal of the shell plate.



Figure 21. Interior Baffle Deformation

While the uppermost portion of the fuel tank exhibited almost no plastic deformation, the portion of the fuel tank below the impact point was bent outward, which caused deformation in the tank mounts. A deformed fuel tank mount is shown in Figure 22.



Figure 22. Deformed Tank Mount

Figure 23 shows the cross-sectional deformation at the impact based on pre- and post-test LIDAR scans. Figure 23 shows both the original and final profiles of the tank taken at a section passing through the point of impact. This figure shows the difference between the initial scan of

the bottom sheet and final resulting dent from the impact to be a depth of approximately 6.3 inches.

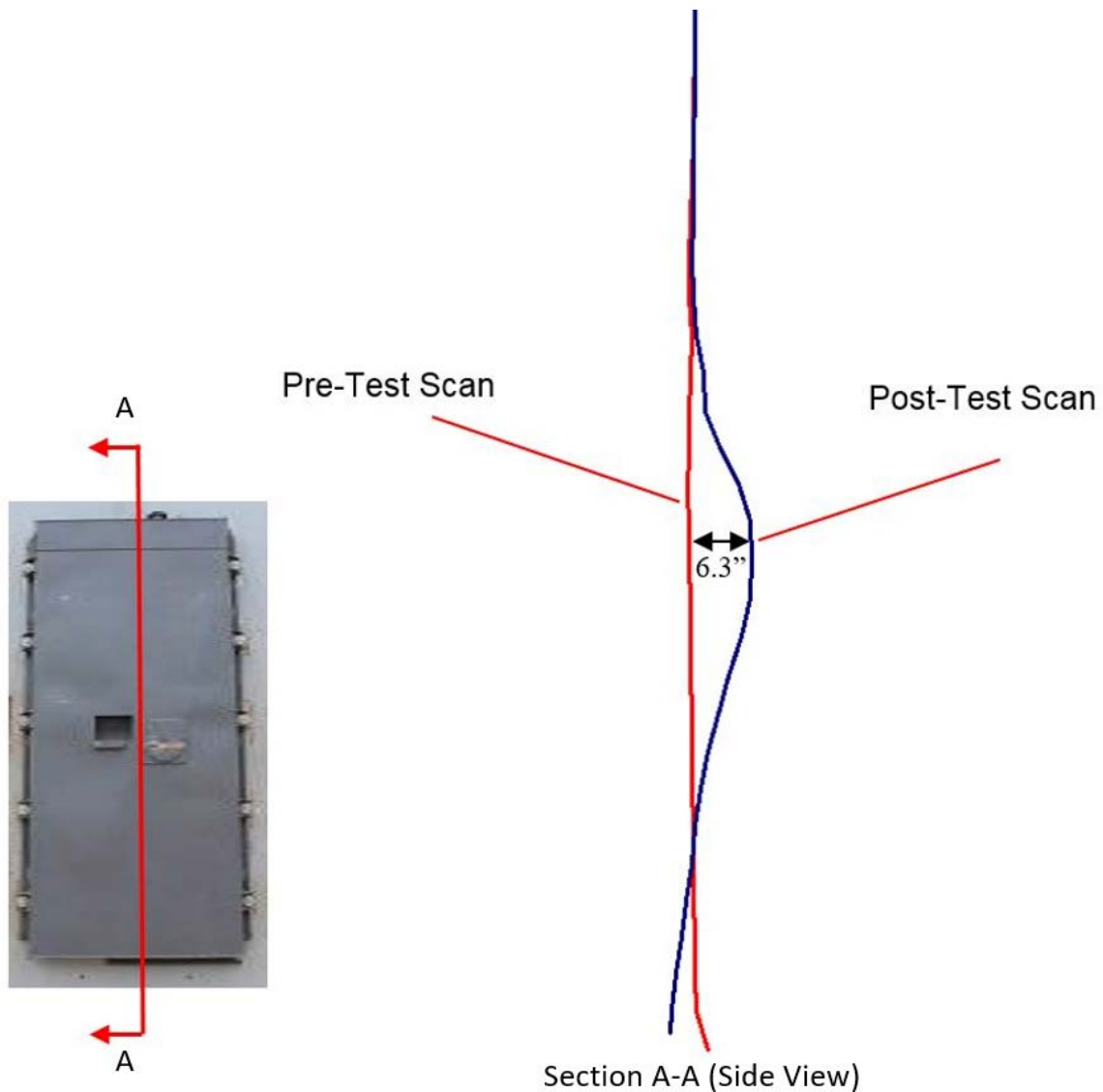


Figure 23. Deformation – Vertical Cross Section at Impact

The average acceleration of the ram cart showed a sustained response reaching a maximum at 12 g's, over a period slightly shorter than 0.1 second. Likewise, the average force of impact showed a sustained response over the same period of time, which reached a maximum at 155,000 pounds. The sustained response of both the average force and the average acceleration was caused by the deformation in the baffles and shell structure, located directly behind the impact point. Figure 24 and Figure 25 show averaged ram cart acceleration in longitudinal direction and force, respectively. TTCI filtered data according to SAE J211 Channel Frequency Class (CFC) 60 [7]. An average was taken from all longitudinal accelerometers, with the exception of BA1CX, which exhibited excessive ringing. BA1CX was located along the centerline of the leading end of the impact cart and recorded acceleration in the x-direction. All data channels are plotted in Appendix B.

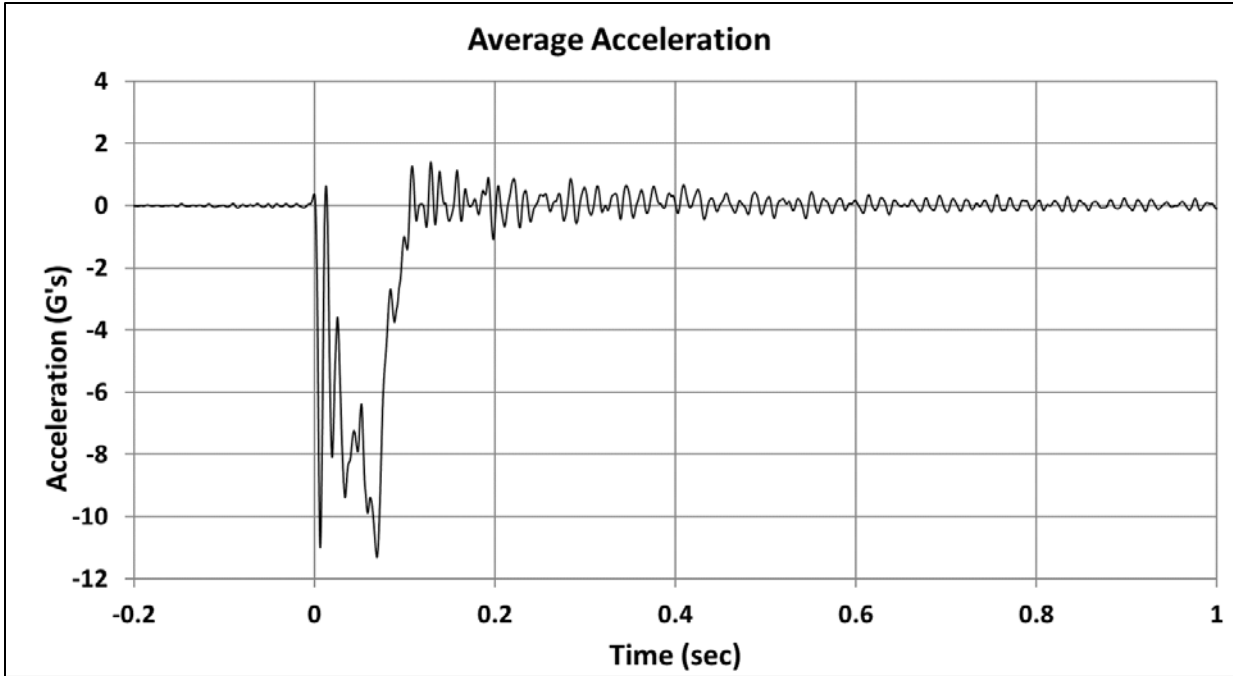


Figure 24. Average Ram Cart Longitudinal Acceleration

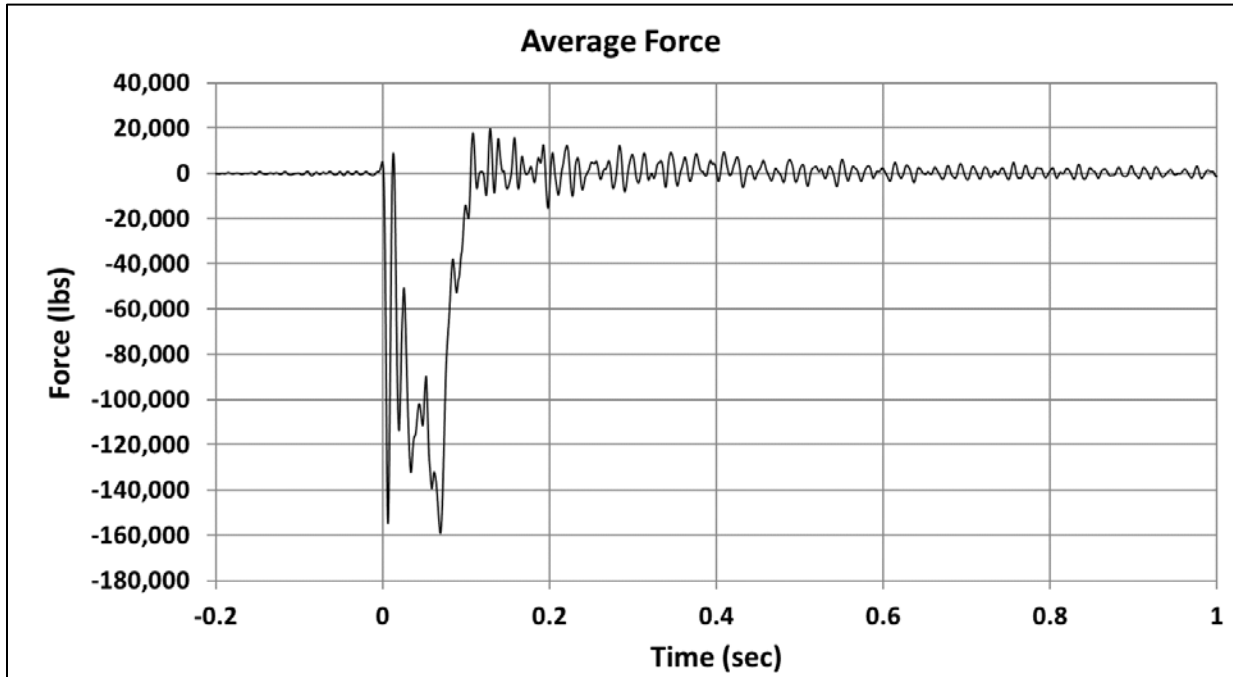


Figure 25. Average Impact Force

4.2 Comparisons Between FE Models and Test Results

Results from three FE models were compared and are discussed in this section. Prior to the test, an FE model using a deformable model of the impact cart was run at 11.1 mph. Also prior to the

test, an FE model using a rigid representation of the impactor with a total mass equal to the impactor, plus the cart was run at 11.5 mph. After the test, a model using the deformable cart and impactor was run at the measured test speed of 11.2 mph.

In general, all the models captured the overall response of the impact event well. Table 6 presents a summary of averaged results from the pre-test FEA and post-test FEA using the deformable impact carts with the measurements from the test. For all test results compared to the FE results throughout this report, the measurements from accelerometer BA1CX have been excluded from the average due to persistent ringing in this channel. Appendix C contains the data from this channel.

Table 6. Comparison of Key Results from Pre-Test FEA, Test, and Post-Test FEA

	Pre-test FEA	Test Data	Post-test FEA
Maximum Impactor Displacement (inches)	8.27 in.	8.19 in.	8.16 in.
Percentage difference	1.0%	-	-0.5%
Peak Impactor Force (kips)	141.5 kips	158.3 kips	173.6 kips
Percentage difference	-10.7%	-	9.6%
Time of Peak Force (seconds)	0.0669 s	0.0692 s	0.0657 s
Percentage difference	-3.4%	-	-5.0%

Figure 26 shows, from left, a post-test photograph of the bottom surface of the tank, a similar view of the deformed tank from the 11.1 mph deformable impactor FEA, the 11.5 mph rigid impactor FEA, and the post-test FEA. In all four images, the outline of the impactor’s corners is apparent in the center of the frame. The indentation pattern is also similar, forming an “X” shaped dent away from the impact zone, toward the sides of the tank.

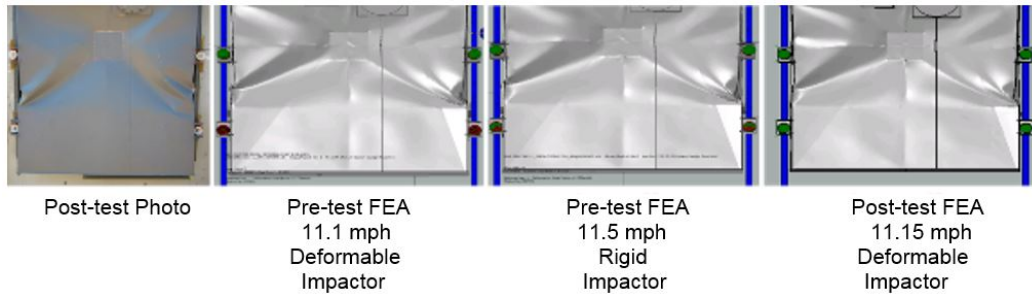


Figure 26. Deformed Bottom Sheet from Post-Test Photo (Left), Pre-Test Model with Deformable Impactor (Second from Left) and Pre-Test Model with Rigid Impactor (Second from Right) and Post-Test Model with Deformable Impactor (Right)

Figure 27 shows, from left, a post-test photograph of the side of the tank at the lowest mounting bracket location, a similar view of the deformed tank from the 11.1 mph deformable impactor FEA, the 11.5 mph rigid impactor FEA, and the post-test FEA. In the test and all three models, the tank experienced a similar response at this mounting bracket. The bottom of the tank (as mounted on the wall) pulled away from the wall during the impact, compressing the rubber bushing as it did. All four images also exhibit a similar area of deformation to the struck surface of the tank in the location adjacent to a bolted-on cover.

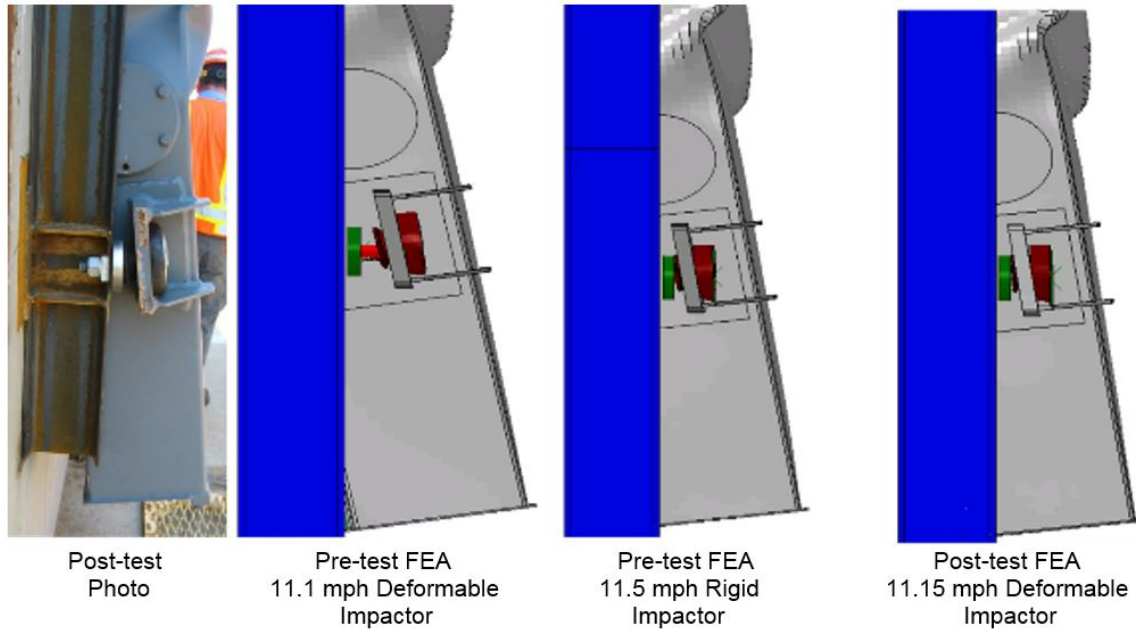


Figure 27. Side View of Deformed Tank Shape from Post-Test Tank (Left), Pre-Test FE Model with Deformable Impactor at 11.1 mph (Center), and Pre-Test FE Model with Rigid Impactor at 11.5 mph (Right)

Following the test, TTCI used a LiDAR-based measurement system to scan the deformed shape of the DMU fuel tank while it was still mounted on the crash wall. This measurement tool was used to create a 3D surface of the deformed tank, which could be compared with the three FE model results. Contours of deformation in the direction of impact are shown in Figure 28 for the post-test geometry of the tank itself, and the three FE models. The surfaces were aligned such that a deformation of 0 inch corresponds to the top of the tank (as mounted on the wall), which was observed to have very little permanent deformation in the FE models. A negative displacement indicates a residual dent (pushed in toward crash wall), while a positive displacement indicates a residual peak (pulled away from crash wall).

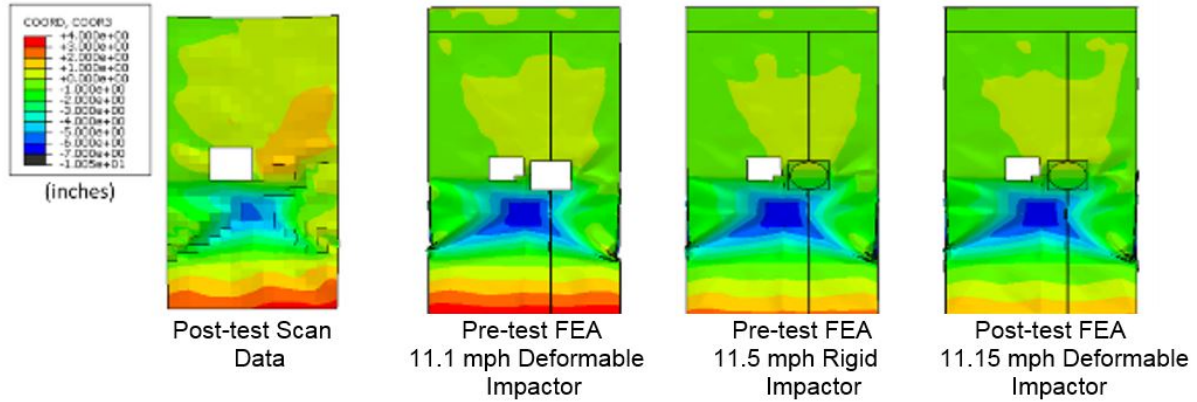


Figure 28. Contour Plots (inches) of Longitudinal Deformation from Post-Test Scan (Left), Pre-Test FE Model with Deformable Impactor at 11.1 mph (Center), and Pre-Test FE Model with 11.5 mph Rigid Impactor (Right)

4.2.1 Pre-Test FE Models

This section presents comparisons between average test data and average results calculated from the pre-test FE models. Individual data channels from the test are compared with corresponding results from the pre-test model using the deformable impact cart in Appendix D.

Figure 29 contains a plot of the force-versus-displacement results from the averaged test data, the pre-test FEA using a 11.5 mph rigid impactor, and the pre-test FEA using an 11.1 mph deformable impactor. The deformable-impactor FEA captures the details of the impact response quite well, including the oscillations measured in the test data. The FEA run using the rigid impactor captures the general force-displacement trend very well, but does not exhibit oscillations to nearly the same degree as the other two results. This indicates that the oscillations are likely attributable to the impact cart used in the test not behaving rigidly.

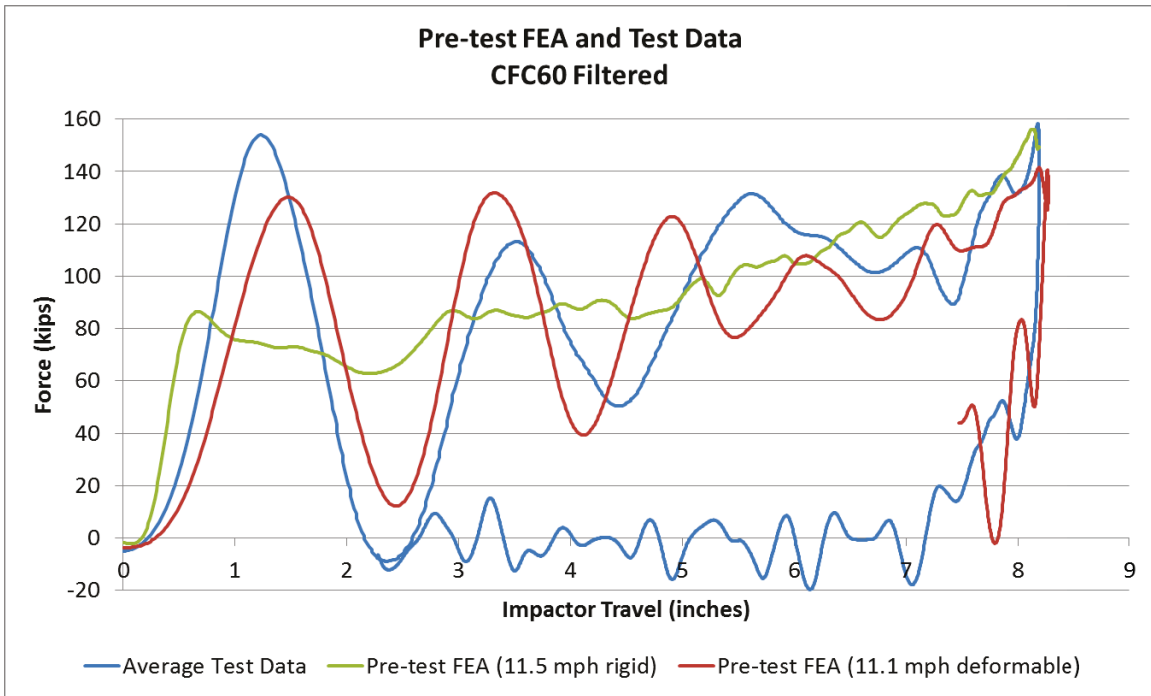


Figure 29. Impactor Force Versus Impactor Travel for Pre-Test FEA and Test Data

Figure 30 contains a comparison of the impactor speed versus time for the pre-test FEA with an 11.5 mph rigid impactor, pre-test FEA with an 11.1 mph deformable impactor, and the test data. All three results are in excellent agreement with one another, and both models capture the time at which the impactor comes to a stop.

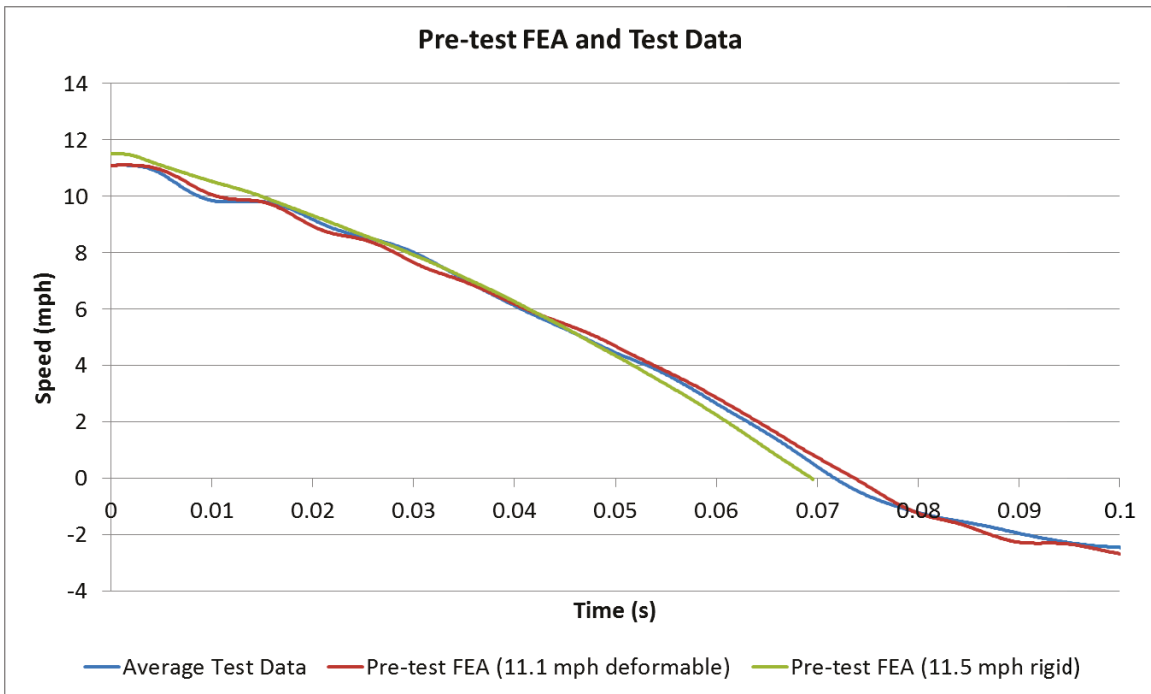


Figure 30. Impactor Speed Versus Time for Pre-Test FEA and Test Data

Figure 31 contains a plot of the impactor travel versus time for the two pre-test FE models and the test data. The three results are in excellent agreement with one another, and all three results indicate a maximum impactor travel of approximately 8.2 inches before rebound begins.

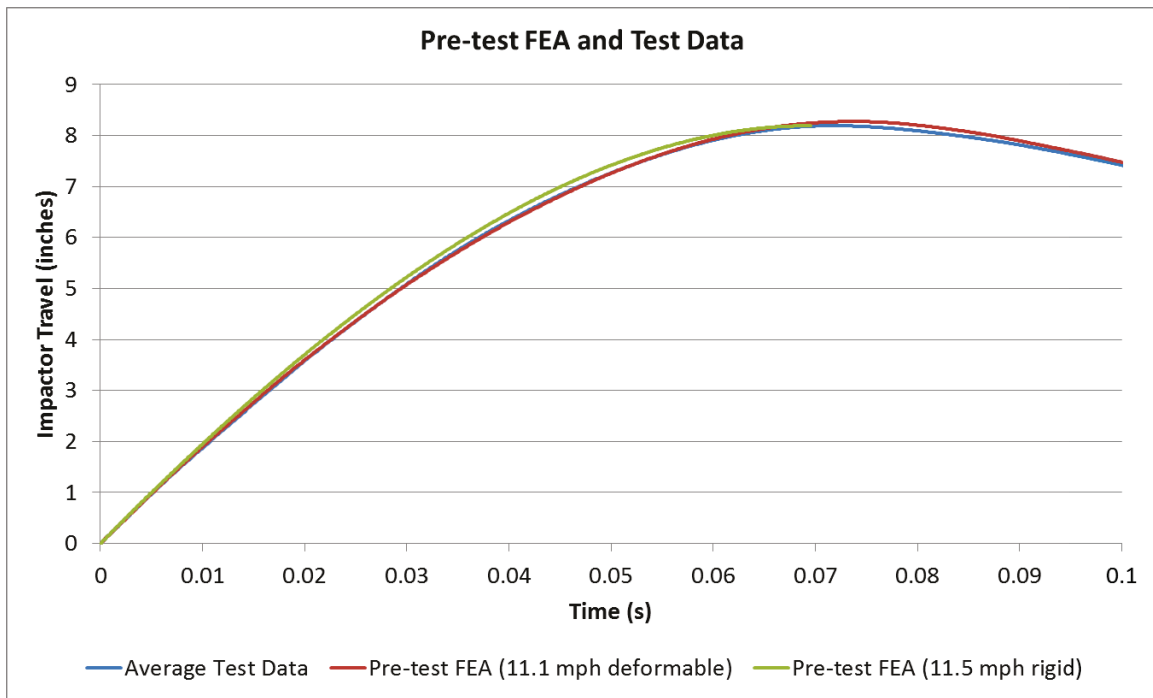


Figure 31. Impactor Travel Versus Time for Pre-Test FEA and Test Data

4.2.2 Post-Test FE Model

This section presents comparisons between average test data and average results calculated from the post-test FE models. Individual data channels from the test are compared with corresponding results from the pre-test model using the deformable impact cart in Appendix D.

The only changes made to the post-test FE model were to give the impact the measured initial velocity of 11.2 mph, improve the refined mesh in the impact zone, and to update the material behaviors to those derived from the sample test data. Figure 32 shows a comparison between the impactor force versus impactor travel for the post-test FEA and the test data. The model continues to exhibit excellent qualitative (shape of the response) and quantitative (magnitude of the response) agreement with the test measurements.

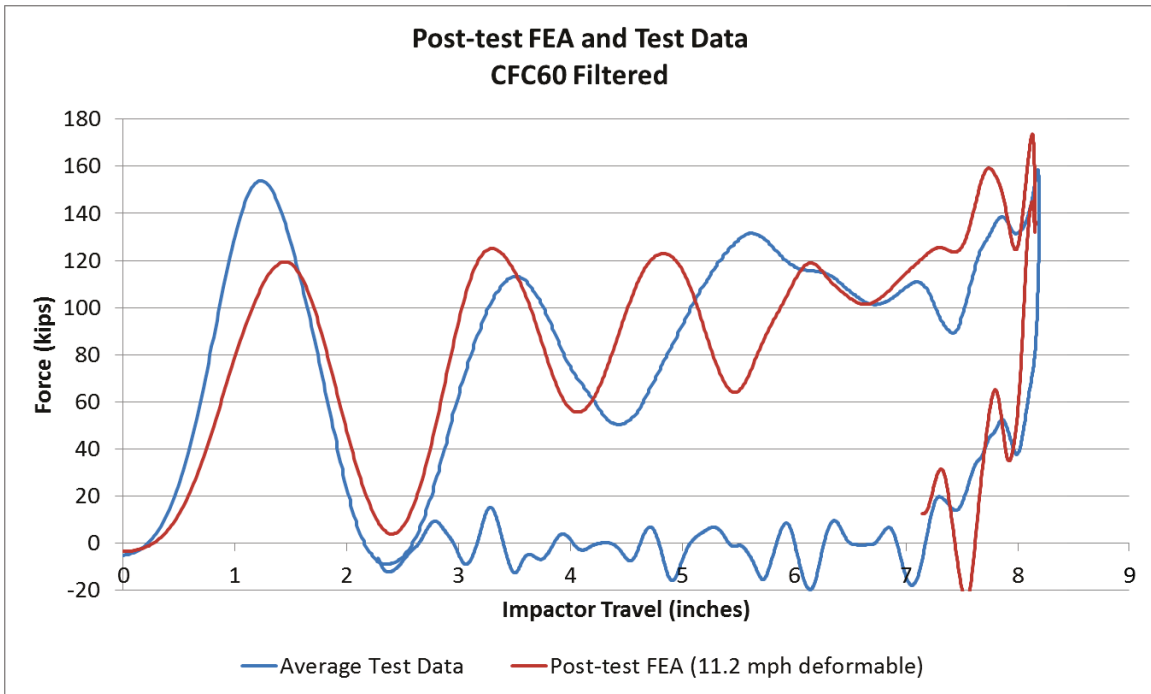


Figure 32. Impactor Force Versus Impactor Travel for Post-Test FEA and Test Data

Figure 33 contains a plot comparing the impactor force versus time for the test data and the post-test FEA. These two responses are in excellent qualitative and quantitative agreement with one another. The model captures the approximate frequency of the oscillatory response, which is likely attributed to deformation of the impact cart itself.

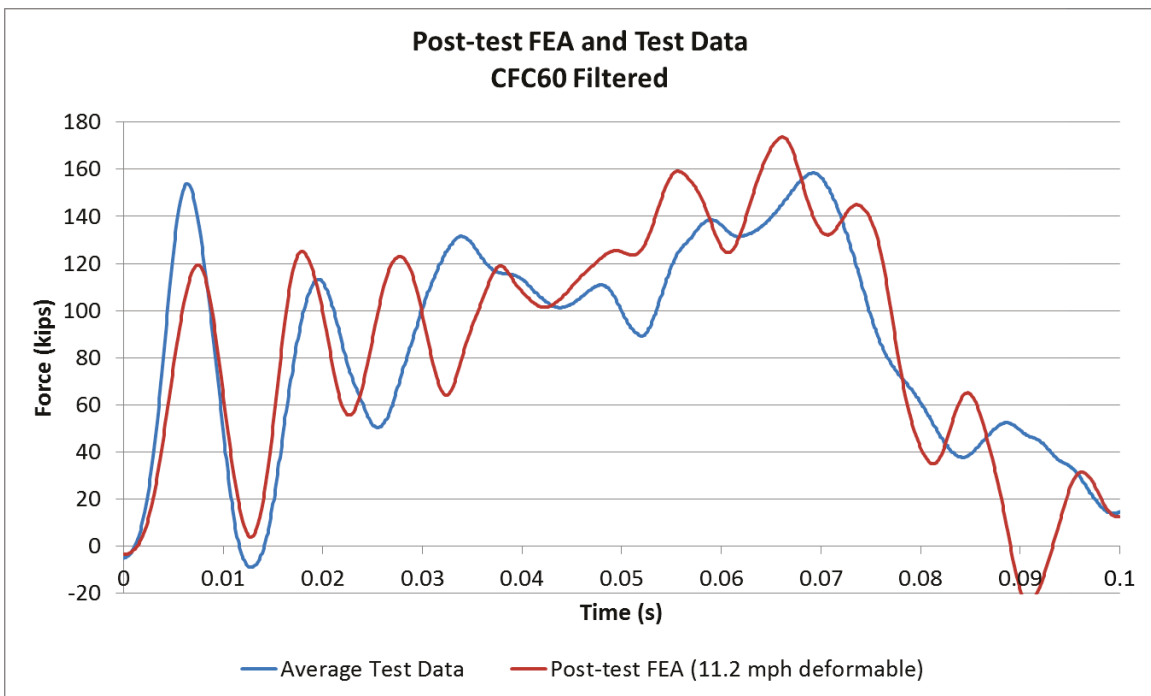


Figure 33. Impactor Force Versus Time for Post-Test FEA and Test Data

Figure 34 contains a comparison of the impactor speed versus time data from the post-test FEA and the test measurements. There is excellent agreement between these results, with both the model and the test impactors coming to a stop shortly after 0.07 second of impact time.

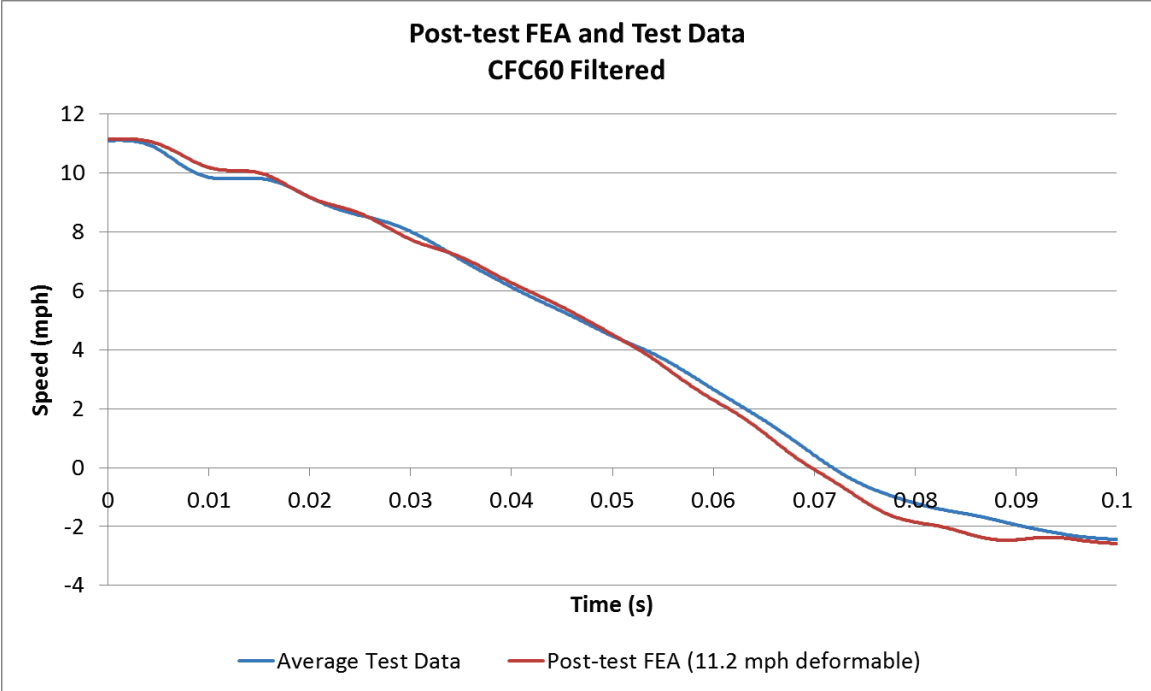


Figure 34. Impactor Speed Versus Time for Post-Test FEA and Test Data

Figure 35 contains a comparison of the impactor travel versus time for both the test data and the post-test FEA. Both results are in excellent agreement, with the impactor reaching a maximum displacement of approximately 8.3 inches before rebounding from the tank.

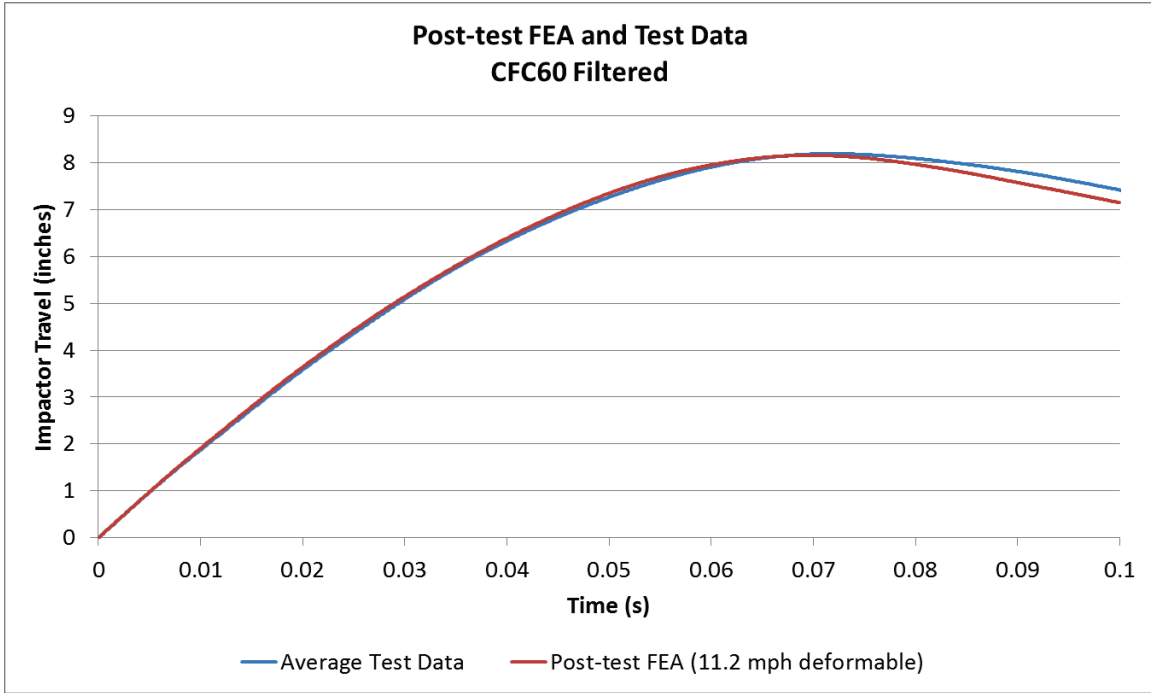


Figure 35. Impactor Travel Versus Time for Post-Test FEA and Test Data

Figure 36 contains a comparison plot between the energy dissipated from the impact cart during the test and from the post-test FEA. For both the test and FEA, the energy was calculated as the area under the respective force-displacement response (Figure 32). This figure shows that the tank successfully absorbed the initial kinetic energy of approximately 58,000 foot-pounds before the impactor rebounded from the tank.

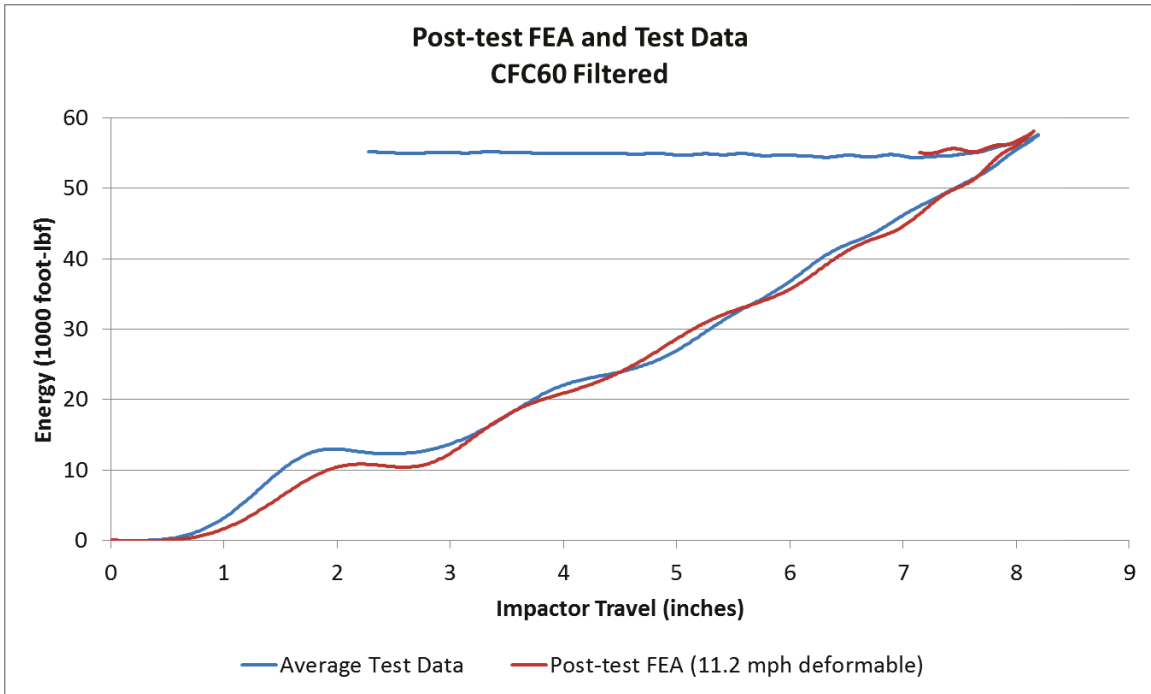


Figure 36. Energy Absorbed by Tank Versus Impactor Travel for Test and Post-Test FEA

Overall, a comparison of results demonstrated the ability of the models to capture the observed modes of deformation of the tank, as well as demonstrated excellent agreement with the measurements made during the test. The model has been validated with the test data, and may be used to simulate impact conditions outside of those in the test.

5. Conclusion

FRA sponsored work performed by TTCI that began on June 28, 2016, at the TTC in Pueblo, CO, of an ongoing dynamic impact test of a DMU fuel tank. The measured speed for this impact test was 11.2 mph, which is below the target speed of 11.5 mph, however, within the pre-test tolerance of ± 2 mph. This impact speed resulted in an impact energy of approximately 58,000 foot-pounds. The impact deformed, but did not puncture the fuel tank. Deformation of the fuel tank during the impact caused permanent deformation of the tank's mounting components. The peak indentation was approximately 8.2 inches, and the fuel tank had a residual deformation of approximately 6.3 inches after the elastic deformation was recovered. Post-test material testing showed that the yield strengths of the fuel tank steels were lower than those used in the initial FEA.

The test successfully measured and recorded the dynamic behavior of the DMU fuel tank in a blunt impact. The DMU fuel tank's material properties and geometry play a significant role in how it deforms under the tested impact conditions. The top and bottom walls of this fuel tank crushed inward before the material could yield enough to tear. Post-test examination of the interior of the tank revealed that the baffles in the area of impact had been crushed nearly solidly between the top and bottom sheets of the fuel tank. The bottom wall of the fuel tank was crushed into the top wall of the tank, which caused additional plastic deformation in areas of the tank away from the impact zone. The fuel tank deformed such that it pulled away from the mounting brackets beneath the impacted zone, which caused deformation in the mounting components. The tank responded to this impact as a single structure, rather than as a bottom sheet acting independently of the rest of the tank structure.

The next phase of full-scale testing is underway to evaluate an oblique impact to fuel tanks, similar to those that can occur in a raking impact to the side or an oblique impact to the bottom or end of the fuel tank. The results of the tensile tests conducted on first DMU fuel tank have been used to update the material behaviors in the FE model, so that future analyses will be more representative of the actual DMU fuel tank behavior. This will assist in planning tests of the remaining two DMU fuel tank specimens. The now-validated FE model of the DMU fuel tank will be used to assist in estimating the response of this type of fuel tank under oblique impact conditions.

6. References

1. Jacobsen, K. (2011, March). “Fuel Tank Crashworthiness: Loading Scenarios.” Paper No. JRC2011-56077. In *Proceedings 2011 Joint Rail Conference*, JRC2011-56077, American Society of Mechanical Engineers. . Available at: http://ntl.bts.gov/lib/37000/37900/37914/JRC2011-56077_Fuel_Tank_Crashworthiness.pdf.
2. Government Publishing Office. Code of Federal Regulations. 49—Transportation Part 229—Railroad Locomotive Safety Standards. Washington, DC. Available at: http://www.ecfr.gov/cgi-bin/text-idx?SID=01e6ba5ad7bf36569b42f6697cd558f7&mc=true&node=se49.4.229_15&rgn=div8.
3. Government Publishing Office. Code of Federal Regulations. 49—Transportation Part 238—Passenger Equipment Safety Standards. Washington, DC. Available at: http://www.ecfr.gov/cgi-bin/text-idx?SID=01e6ba5ad7bf36569b42f6697cd558f7&mc=true&node=se49.4.238_15&rgn=div8.
4. Carolan, M., Rakoczy, P., and Jacobsen, K. (2017, August 16). “Blunt Impact Tests of Retired Passenger Locomotive Fuel Tanks.” U.S. Department of Transportation, DOT/FRA/ORD-17/11. Available at: <https://www.fra.dot.gov/eLib/details/L18819>.
5. Jacobsen, K., Carolan, M., Perlman, A.B. (2014, April). “Conventional Fuel Tank Blunt Impact Tests: Test and Analysis Results.” In *Proceedings of the 2014 Joint Rail Conference*, JRC2014-3786, American Society of Mechanical Engineers. Available at: <http://ntlsearch.bts.gov/tris/record/ntl/51599.html>.
6. Jacobsen, K., Carolan, M. (2015, March). “Results of a Conventional Fuel Tank Blunt Impact Test.” In *Proceedings 2015 Joint Rail Conference*, JRC2015-5759. American Society of Mechanical Engineers. Available at: <http://ntlsearch.bts.gov/tris/record/ntl/54927.html>.
7. SAE International. (2007). Standard J211-1. “Instrumentation for Impact Test – Part 1 – Electronic Instrumentation.” Available at: http://standards.sae.org/j211/1_199503/.
8. Dassault Systèmes Simulia Corp. (2014). Abaqus Version 6.14-2, Performance Benchmark and Profiling: Providence, RI.
9. Hechler, O., Axmann, G., and Donnay, B. (2009, June 26). *The Right Choice of Steel – According to the Eurocode*. ArcelorMittal. Luxembourg. Available at: http://sections.arcelormittal.com/uploads/tx_abdownloads/files/25_The_right_choice_of_steel_Ver2.pdf.
10. Lee, Y.W., and Wierzbicki, T. (2004, August). “Quick Fracture Calibration for Industrial Use.” Impact & Crashworthiness Laboratory Report No. 115, Massachusetts Institute of Technology.

Appendix A – Instrumentation Locations and Technical Specification

Video Setup

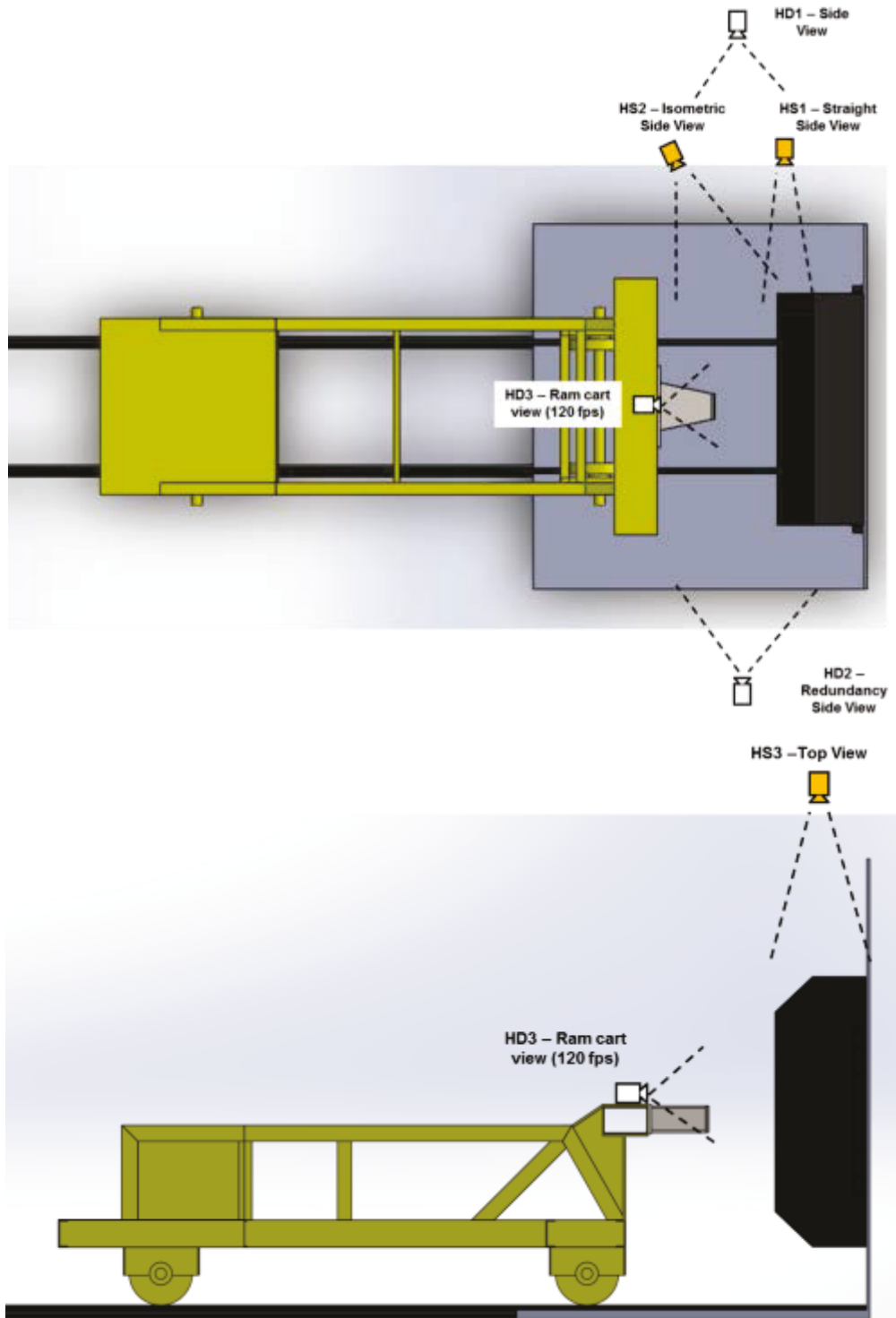


Figure A1. Camera Views

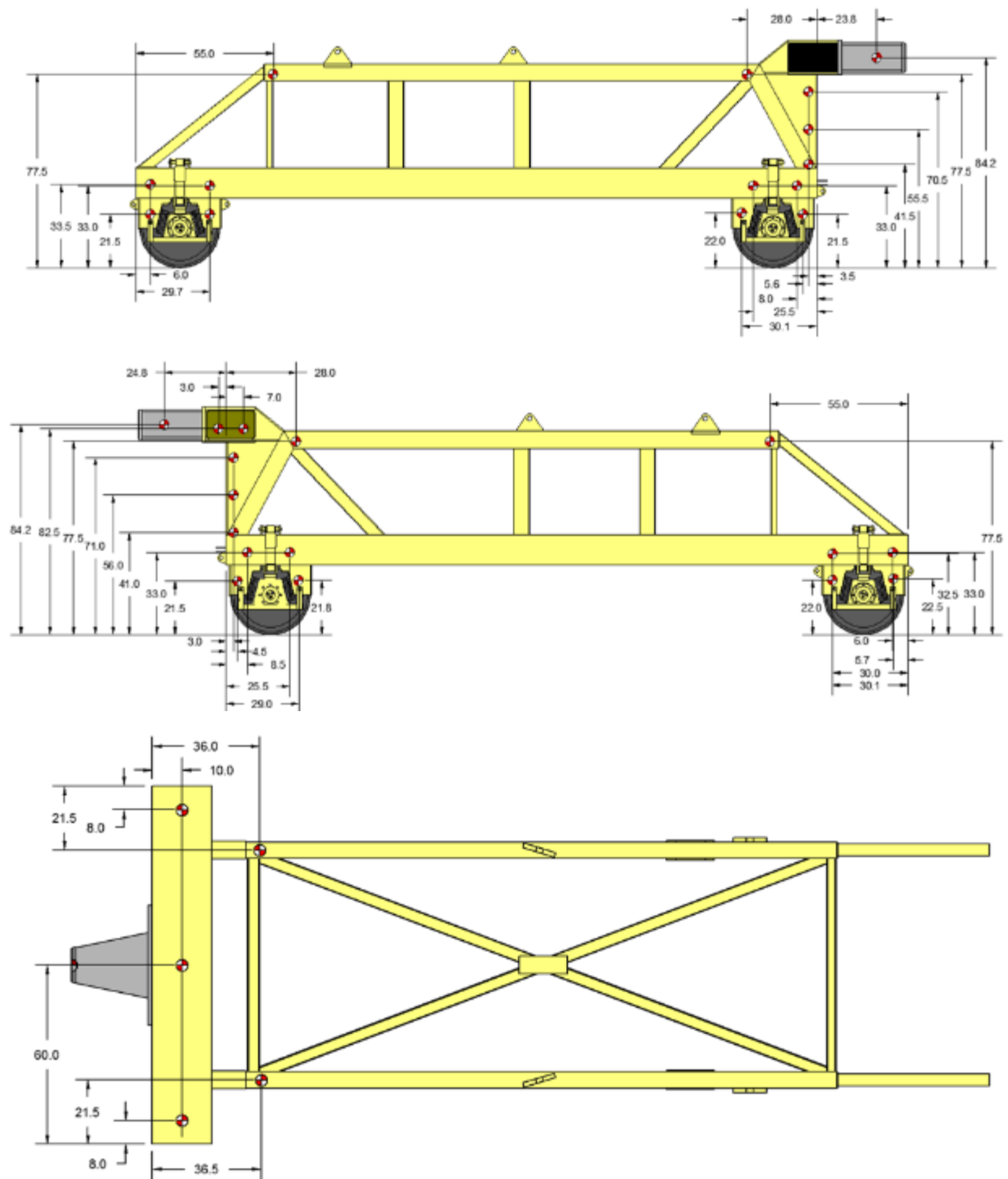


Figure A2. Impact Cart Target Locations

Appendix B – Fuel Tank Materials

Pre-Test Material Modeling

Because excising samples from the fuel tank to be used in tensile testing could compromise the structure, pre-test material modeling was not based on measurements on the actual tank. The information provided with the tanks included identification of the materials used to construct various components. For the structures of the tank expected to undergo permanent deformation in the test, the plastic stress-strain response of each material needed to be defined in the FE models. The plastic response of each material in the tank was estimated from curves for similar materials to those used in the construction of the tank [9]. This reference published nominal (engineering) stress-strain responses materials referred to as S235 and S355. While not identical to the materials of construction of the fuel tank, these published curves were expected to provide a reasonable representation of the materials of construction, suitable for the pre-test model to estimate the test response.

A series of discrete, regularly-spaced stress-strain points were manually fit to each curve. The Abaqus/Explicit FE software offers several approaches to modeling metal plasticity. Using an isotropic hardening approach, metal plasticity is defined using true plastic strain and true stress. Therefore, the engineering stress and engineering strain results must be transformed using equations B1 and B2 before being used as an input in the FE model.

$$\sigma_{true} = \sigma_{nom}(1 + \epsilon_{nom}) \quad (B1)$$

$$\epsilon_{ln}^{pl} = \ln(1 + \epsilon_{nom}) - \frac{\sigma_{true}}{E} \quad (B2)$$

The true stress, true plastic strain behaviors defined in the pre-test model are shown in Figure B1.

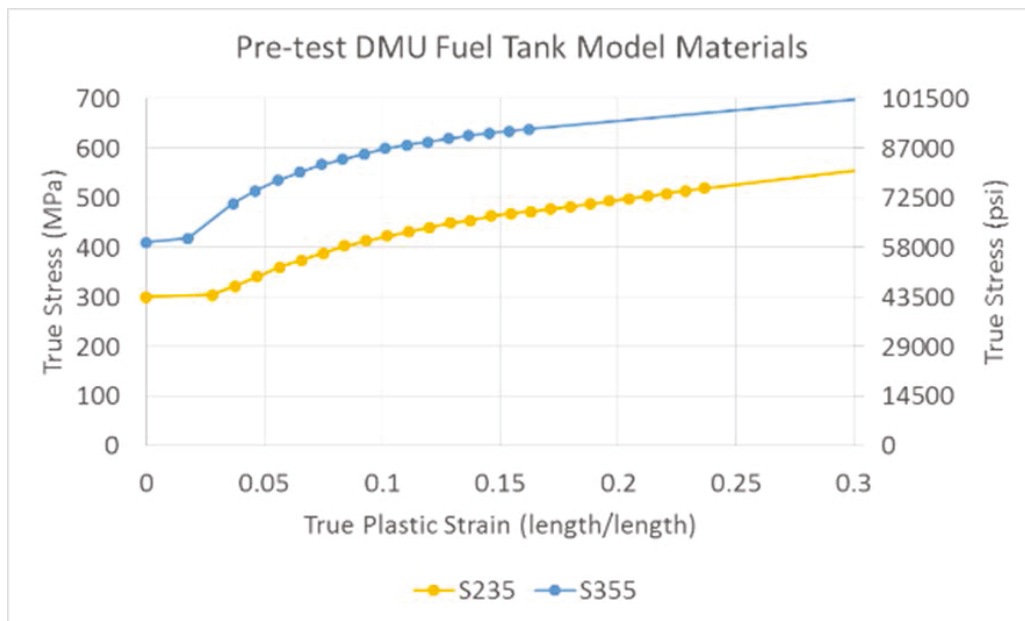


Figure B1. True Stress, True Plastic Strain for Pre-Test Materials

The true plastic strains and true stresses for S235 and S355 used in the pre-test models are given in Tables B1 and B2, respectively.

Table B1. Stress-Strain Behavior Input to Pre-Test Model for S235

True Plastic Strain (in/in)	True Stress (MPa)	True Stress (psi)
0	300	43,511
0.0280	303.85	44,070
0.0376	322.4	46,760
0.0471	341.25	49,494
0.0565	360.4	52,272
0.0658	374.5	54,317
0.0750	388.8	56,391
0.0842	403.3	58,494
0.0932	413.6	59,988
0.1022	422.91	61,338
0.1112	431.2	62,540
0.1200	440.7	63,918
0.1288	449.16	65,145
0.1375	454.25	65,884
0.1461	462.84	67,129
0.1547	468	67,878
0.1632	472	68,458
0.1716	477.19	69,211
0.1799	482.4	69,966
0.1882	487.63	70,725
0.1964	492.88	71,486
0.2045	498.15	72,251
0.2126	503.44	73,018
0.2206	508.75	73,788
0.2285	514.08	74,561
0.2364	519.43	75,337
1	950	137,786

Table B2. Stress-Strain Behavior Input to Pre-Test Model for S355

True Plastic Strain (in/in)	True Stress (MPa)	True Stress (psi)
0	410	59,466
0.0177	418.2	60,655
0.0368	488.8	70,895
0.0462	514.5	74,622
0.0556	535.3	77,639
0.0649	551.05	79,923
0.0741	567	82,237
0.0833	577.7	83,788
0.0924	588.5	85,355
0.1014	599.4	86,936
0.1103	605.92	87,881
0.1192	612.46	88,830
0.1279	619.02	89,781
0.1366	625.6	90,736
0.1453	629.88	91,357
0.1538	634.14	91,974
0.1623	638.38	92,589
1	1000	145,038

In addition to the elastic-plastic material behavior, a constant plastic strain to failure of 0.4 was defined for each material in the pre-test models. Regardless of the triaxiality of the stresses within the element, if the plastic equivalent strain reached 0.4, the element would begin to fail and be removed from the mesh. This simple approach to modeling puncture was expected to be replaced with a more sophisticated, triaxiality-based failure characterization in the post-test model once sample data were available to develop the failure response.

Material Coupon Data

Material samples were cut from various structures on the DMU fuel tank after the impact test. The nominal (engineering) stress-strain responses from each tested material are presented in Figures B1 through B3. Three samples of each material were tested. Results from the material tests are shown in Figures B4 through B8.

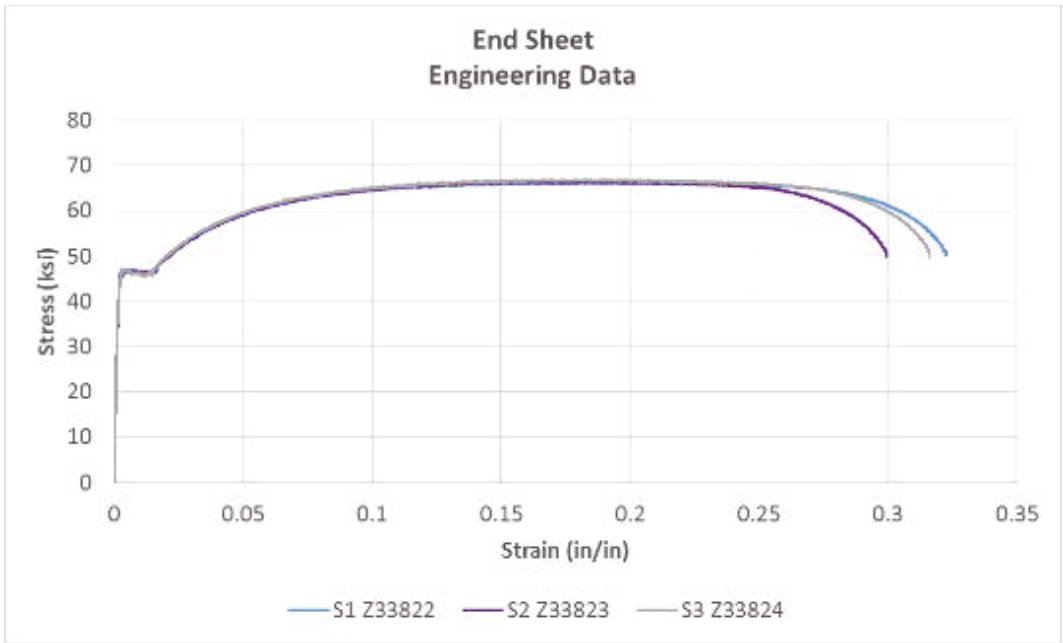


Figure B2. Engineering Stress-Strain Responses from DMU Tank End Sheet Samples

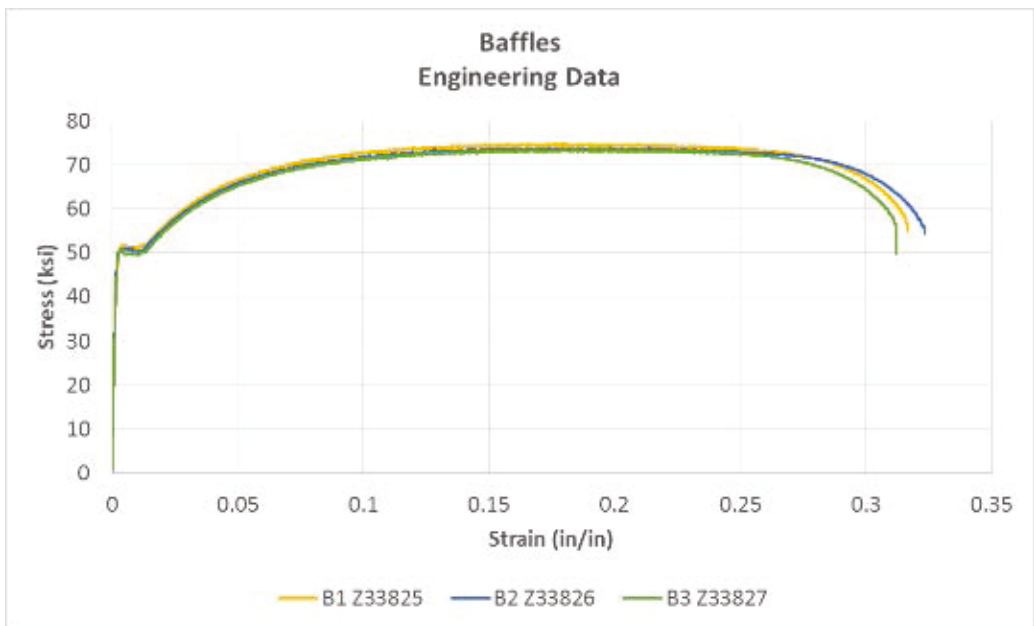


Figure B3. Engineering Stress-Strain Responses from DMU Tank Baffle Samples

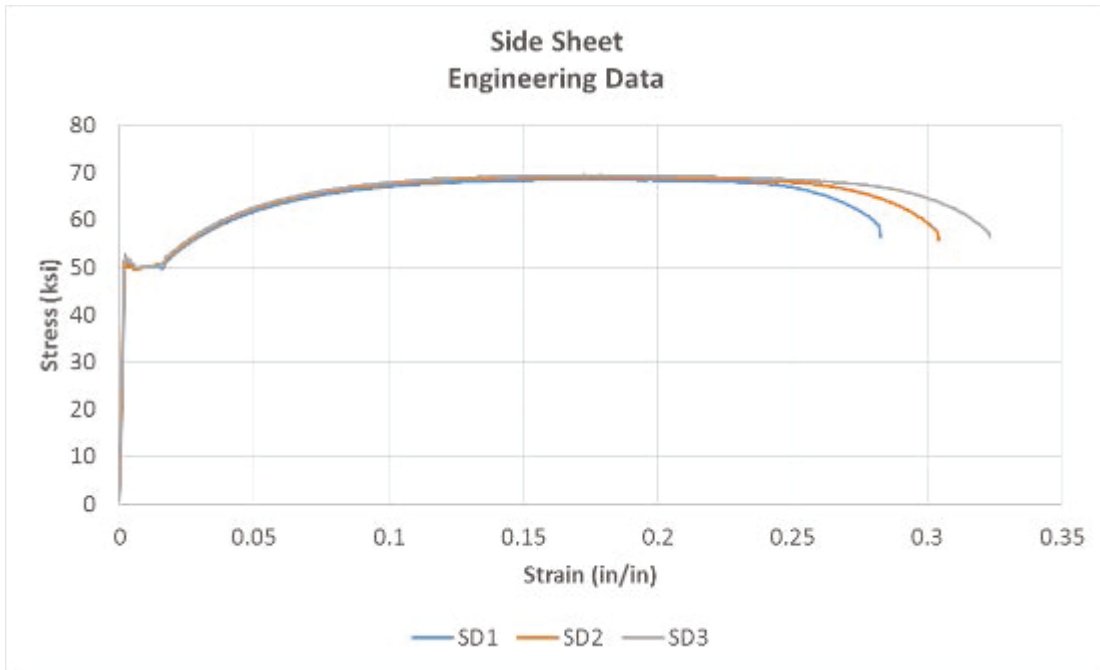


Figure B4. Engineering Stress-strain Responses from DMU Tank Side Sheet Samples



Westmoreland Mechanical Testing & Research, Inc.
 P.O. Box 388; 221 Westmoreland Drive
 Youngstown, PA 15696-0388 U.S.A.
 Telephone: 724-537-3131 Fax: 724-537-3151
 Website: www.wmtr.com E-Mail: admin@wmtr.com
 WMT&R is a technical leader in the material testing industry.



CERTIFICATION

August 4, 2016
 Transportation Technology Center Inc.
 55500 DOT Road
 P.O. Box 11130
 Pueblo, CO 81001

Section 1 of 1

WMT&R Report No. 6-67135
 P.O. No. 31815
 WMT&R Quote No. QN162875 Rev.1

Attention: Travis Gorham

Subject: All processes, performed upon the material as received, were conducted at WMT&R, Inc. in accordance with the WMT&R Quality Assurance Manual, Rev. 11, dated 12/03/2008.
 The following tests were performed on this order: TENSILE

TENSILE RESULTS: ASTM E8-15a

SPEED OF TESTING: 0.005 in./in./min., Extensometer travel exceeded - Test continued at last stroke rate

MATERIAL: CARBON STEEL

DISPOSITION: Report

SID	TestLog Number	Temp.	UTS ksi	0.2% YS ksi	Elong %	Modulus Msi	Ult. Load lbf	0.2% YLD. lbf	Orig. Width (in.)	Orig. Thick (in.)	4D Orig GL (in.)	4D Final GL (in.)	Orig. Area (sq. in.)	Machine Number	A/U/R
S1	Z33822	Room	66.5	46.6	34	30.9	4277	2997	0.5030	0.1278	2.00	2.67	0.06428340	M26	R
S2	Z33823	Room	66.7	46.0	31	29.9	4277	2953	0.5028	0.1276	2.00	2.61	0.06415728	M26	R
S3	Z33824	Room	66.9	46.8	33	29.9	4293	2999	0.5027	0.1276	2.00	2.66	0.06414452	M26	R
B1	Z33825	Room	74.8	51.5	32	29.6	4478	3084	0.5034	0.1190	2.00	2.64	0.05990460	M26	R
B2	Z33826	Room	73.9	51.0	34	29.3	4424	3052	0.5031	0.1190	2.00	2.68	0.05986890	M26	R
B3	Z33827	Room	73.7	50.8	33	29.6	4416	3045	0.5030	0.1192	2.00	2.65	0.05995760	M26	R

A/U/R: A=ACCEPTABLE, U=UNACCEPTABLE, R=REPORT

NOTE: THE RECORDING OF FALSE, FICTITIOUS OR FRAUDULENT STATEMENTS OR ENTRIES ON THIS DOCUMENT MAY BE PUNISHABLE AS A FELONY UNDER FEDERAL STATUTE. THIS CERTIFICATE OR REPORT SHALL NOT BE REPRODUCED EXCEPT IN FULL WITHOUT THE WRITTEN APPROVAL OF WMT&R, INC.

Signature Redacted

Tensile Supervisor

August 4, 2016

Testing Specialists for Aerospace, Automotive, and Material Testing Fields
 Locations in Youngstown, PA U.S.A. ~ Tel. (724) 537-3131 and
 Banbury, Oxon U.K. ~ Tel. +44 (0) 1295 261211



Figure B5. Results from Material Tests

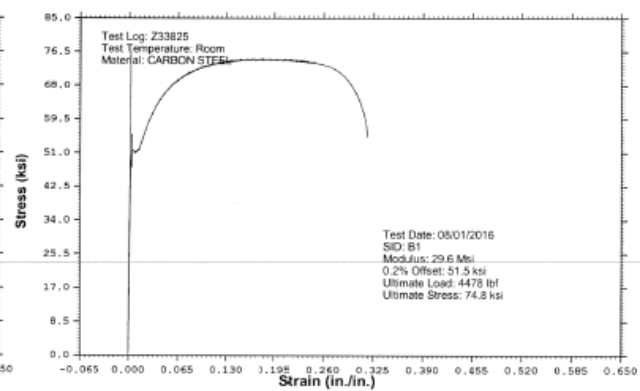
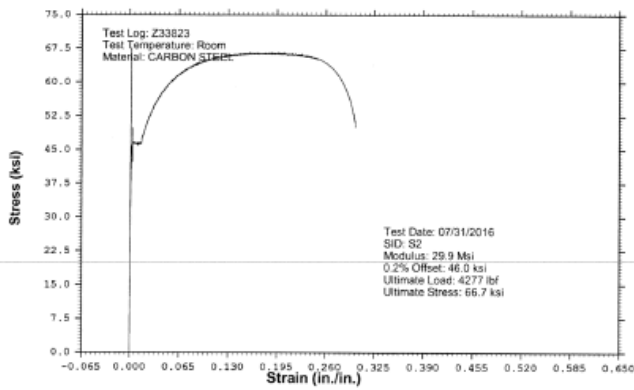
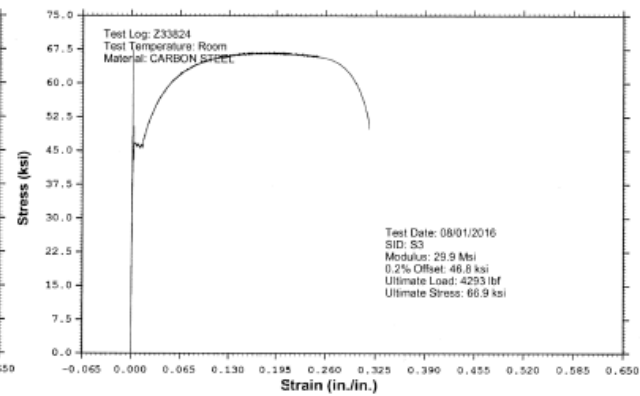
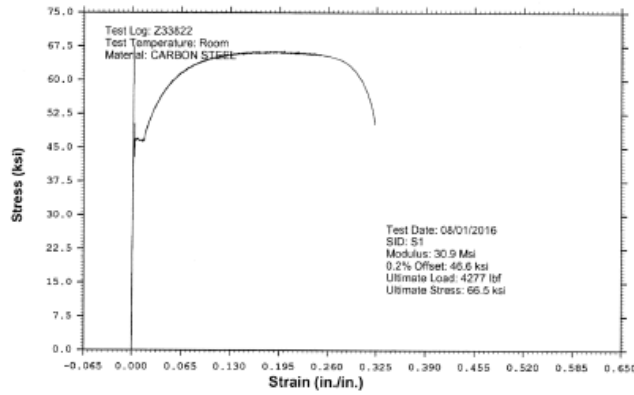
WESTMORELAND MECHANICAL TESTING & RESEARCH, Inc

Stress vs. Strain

Phone: (724)537-3131

Customer: Transportation Technology Center Inc.
WMT&R Report: 6-67135

P.O. No.: 31815
WMT&R Quote No.: QN162875 Rev.1



"NOTE: THE RECORDING OF FALSE, FICTITIOUS OR FRAUDULENT STATEMENTS OR ENTRIES ON THIS DOCUMENT
MAY BE PUNISHABLE AS A FELONY UNDER FEDERAL STATUTE."

Figure B6. Results from Material Tests

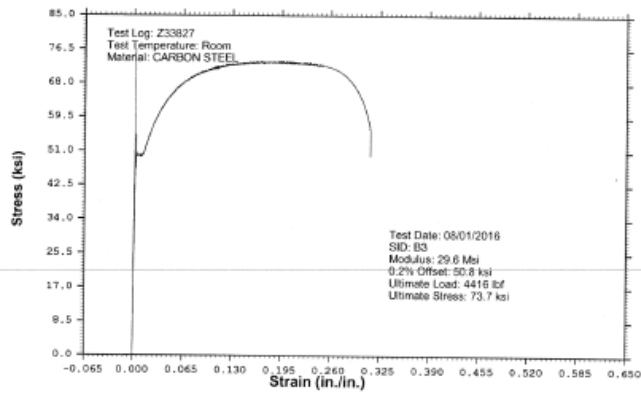
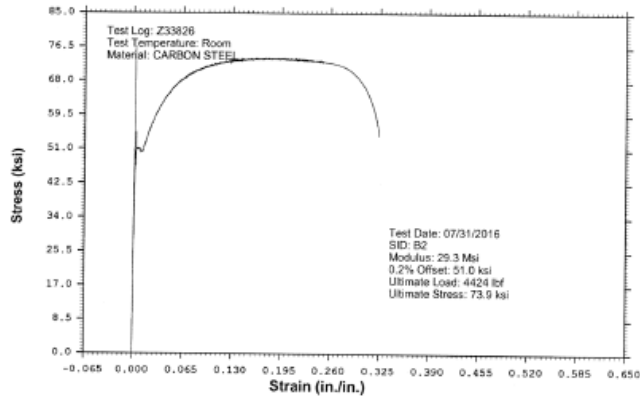
WESTMORELAND MECHANICAL TESTING & RESEARCH, Inc

Stress vs. Strain

Phone: (724)537-3131

Customer: Transportation Technology Center Inc.
WMT&R Report: 6-67135

P.O. No.: 31815
WMT&R Quote No.: QN162875 Rev.1



*NOTE: THE RECORDING OF FALSE, FICTITIOUS OR FRAUDULENT STATEMENTS OR ENTRIES ON THIS DOCUMENT
MAY BE PUNISHABLE AS A FELONY UNDER FEDERAL STATUTE.*

Figure B7. Results from Material Tests



Westmoreland Mechanical Testing & Research, Inc.
 P.O. Box 388; 221 Westmoreland Drive
 Youngstown, PA 15696-0388 U.S.A.
 Telephone: 724-537-3131 Fax: 724-537-3151
 Website: www.wmtr.com E-Mail: admin@wmtr.com
WMT&R is a technical leader in the material testing industry.



CERTIFICATION

November 23, 2016
 Transportation Technology Center Inc.
 55500 DOT Road
 P.O. Box 11130
 Pueblo, CO 81001

Section 1 of 1
WMT&R Report No. 6-76647
 P.O. No. 32131
 WMT&R Quote No. QN154748

Attention: Travis Gorhum

Subject: All processes, performed upon the material as received, were conducted at WMT&R, Inc. in accordance with the WMT&R Quality Assurance Manual, Rev. 11, dated 12/03/2008.
 The following tests were performed on this order: TENSILE

TENSILE RESULTS: ASTM E8-16a
SPEED OF TESTING: 0.005 in./in./min.
MATERIAL: Steel

DISPOSITION: Report

SID	TestLog Number	Temp.	UTS ksi	0.2% YS ksi	Elong %	RA %	Modulus Msi	Ult. Load lbf	0.2% YLD. lbf	Orig. Width (in.)	Final Width (in.)	Orig. Thick (in.)	Final Thick (in.)	4D Orig GL (in.)	4D Final GL (in.)	Orig. Area (sq. in.)	Machine Number	AU/R
Sd1	05206H	Room	68.6	50.7	29	54	25.0	4378	3235	0.5032	0.3801	0.1268	0.0770	2.00	2.57	0.06380576	M10	R
Sd2	05207H	Room	69.2	50.2	31	54	27.6	4389	3186	0.5026	0.3712	0.1262	0.0763	2.00	2.62	0.06342612	M10	R
Sd3	05208H	Room	69.6	51.7	32	55	29.8	4404	3274	0.5040	0.3711	0.1256	0.0769	2.00	2.64	0.06330240	M10	R

AU/R: A=ACCEPTABLE, U=UNACCEPTABLE, R=REPORT

Signature Redacted

Tensile Supervisor

November 23, 2016

NOTE: THE RECORDING OF FALSE, FICTITIOUS OR FOLLOKMENT STATEMENTS OR ENTRIES ON THIS DOCUMENT MAY BE PUNISHABLE AS A FELONY UNDER FEDERAL STATUTE! THIS CERTIFICATE OR REPORT SHALL NOT BE REPRODUCED EXCEPT IN FULL WITHOUT THE WRITTEN APPROVAL OF WMT&R.

Testing Specialists for Aerospace, Automotive, and Material Testing Fields
 Locations in Youngstown, PA U.S.A. - Tel. (724) 537-3131 and
 Banbury, Oxon U.K. - Tel. +44 (0) 1295 261211



Figure B8. Results from Material Tests

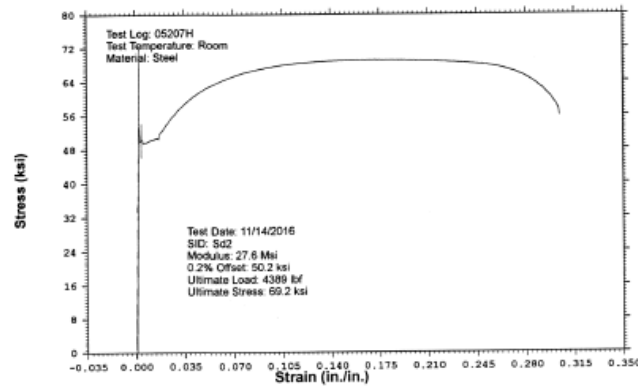
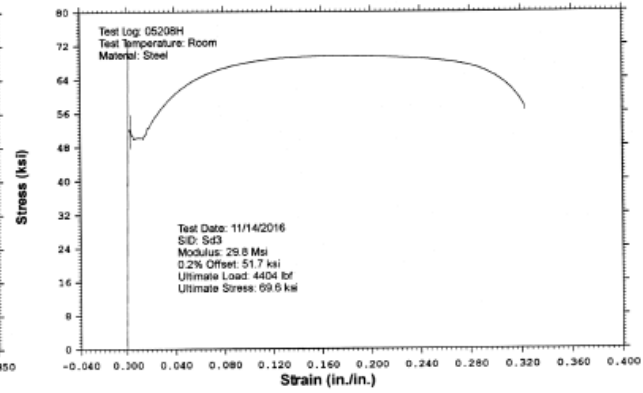
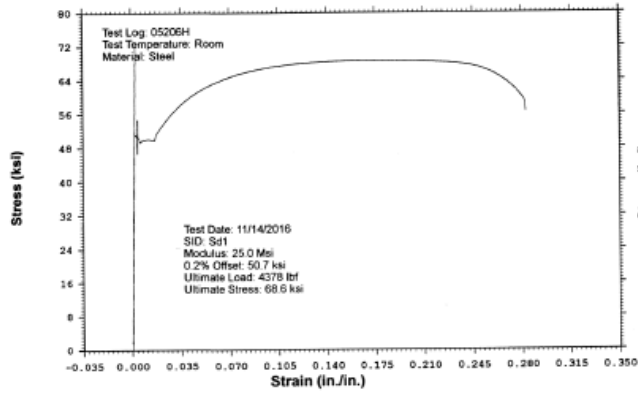
WESTMORELAND MECHANICAL TESTING & RESEARCH, Inc

Stress vs. Strain

Phone: (724)537-3131

Customer: Transportation Technology Center Inc.
WMT&R Report: 6-76647

P.O. No.: 32131
WMT&R Quote No.: QN164748



"NOTE: THE RECORDING OF FALSE, FICTITIOUS OR FRAUDULENT STATEMENTS OR ENTRIES ON THIS DOCUMENT
MAY BE PUNISHABLE AS A FELONY UNDER FEDERAL STATUTE."

Figure B9. Results from Material Tests

Material Modeling in Abaqus/Explicit

The general approach used to develop material models was to simulate the tensile sample tests that were performed on the end sheet, side sheet, and baffles materials cut from the DMU fuel tank. This appendix describes the development and execution of the sample FE models, as well as the development of the material parameters used in the post-test models.

Half-symmetric solid FE models were created for the end sheet and baffle tensile samples, and a quarter-symmetric shell FE model was created for the side sheet tensile sample as illustrated in Figure B10. A displacement boundary condition was applied to the top end of the sample in the positive Z direction at a constant rate of 2.5 in/s for the half-symmetric models and 1.25 in/s for the quarter-symmetric model until fracture occurred. The Abaqus/Explicit solver was used with a time period of 0.5s, and it was observed that a quasi-static state was maintained. The end sheet and baffle samples were meshed using incompatible mode eight-node brick elements (C3D8I) inside the gage region and reduced integration eight-node brick elements (C3D8R) outside the gage. Both the C3D8I and C3D8R elements had a size of 0.0319 inch corresponding to four elements across the full thickness of the sample. The side sheet samples were meshed using four-node shell elements (S4) inside the gage region and reduced integration four-node shell elements (S4R) outside the gage region. The shell elements had a size of 0.0625 inch corresponding to five elements across half the width of the gage. A linear spring with a negligible stiffness (1×10^{-6} lbf/inch) was placed across the center of the 2-inch gage region to act as an extensometer to measure engineering strain. A zero displacement boundary condition was applied to the bottom face of the sample in the Z direction, and the reaction force was summed to calculate engineering stress.

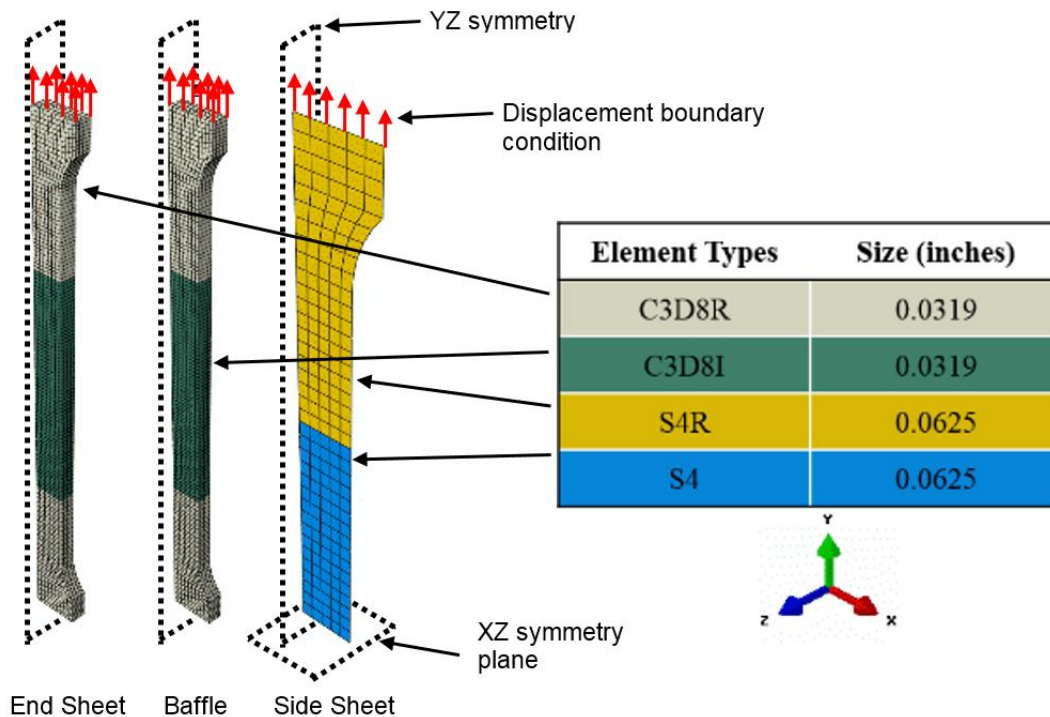


Figure B10. Uniaxial Tensile Sample FE Model

For all post-test material models defined for the DMU fuel tank, the value of Young’s modulus obtained from the tensile testing was used in the model. Those values are summarized in Table B3.

Table B3. Values of Young’s Modulus Used in Post-Test FE Models

	Young’s Modulus (psi)	Young’s Modulus (MPa)
End Sheet	27,466,666	189,376
Baffles	29,600,000	204,085
Side Sheet	29,900,000	206,153

In addition to converting the data into the format used in Abaqus, the test data were reduced and regularized into 14 points up to the ultimate tensile strength (UTS) for each section material. A 15th point was then linearly extrapolated at a non-physical, large strain of 1 in/in. Three post-test true stress-strain curves corresponding to the three FE tensile samples that were modeled are shown in Figure B11. This figure also includes the input data that was used for the pre-test baffle and outer sheet materials, for reference. An iterative approach was taken to scale the input true stress values in order to reach better agreement with the UTS measured from the sample tensile test. It was found that the input true stress for the side sheet material did not require scaling, however, both the end sheet and baffle input true stress data were scaled by a factor of 1.05 outside the region of true strain dominated by the formation of Lüders bands.

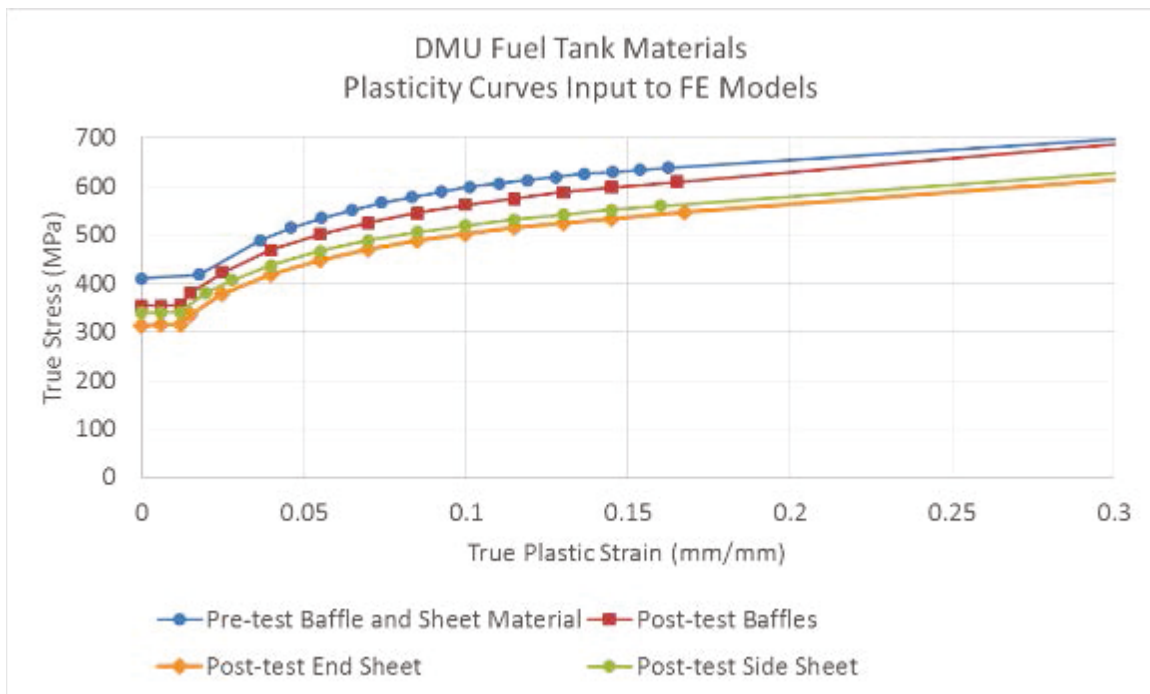


Figure B11. True Stress, True Plastic Strain Input Curves for Pre- and Post-Test FE Models

Tabular values for the true plastic strain and true stress responses defined for the end sheet, baffles, and side sheet in the post-test models are provided in Tables B4 through B6, respectively.

Table B4. Stress-Strain Behavior Input to Post-Test FE Models for End Sheet Material

True Plastic Strain (in/in)	True Stress (MPa)	True Stress (psi)
0.0000	313.71	45,500
0.0060	314.40	45,600
0.0120	315.09	45,700
0.0150	334.40	48,500
0.0250	377.47	54,748
0.0400	418.08	60,638
0.0550	448.02	64,980
0.0700	470.98	68,309
0.0850	487.34	70,682
0.1000	501.55	72,743
0.1150	514.36	74,601
0.1300	525.11	76,161
0.1450	534.12	77,467
0.1675	546.95	79,328
1.0000	964.68	139,914

Table B5. Stress-Strain Behavior Input to Post-Test FE Models for Baffle Material

True Plastic Strain (in/in)	True Stress (MPa)	True Stress (psi)
0.0000	353.70	51,300
0.0060	354.39	51,400
0.0120	355.08	51,500
0.0150	379.54	55,047
0.0250	422.84	61,328
0.0400	469.02	68,026
0.0550	501.54	72,743
0.0700	525.24	76,179
0.0850	545.35	79,096
0.1000	561.59	81,451
0.1150	574.63	83,343
0.1300	587.96	85,277
0.1450	597.59	86,673
0.1652	609.53	88,405
1.0000	1094.01	158,673

Table B6. Stress-Strain Behavior Input to Post-Test FE Models for Side Sheet Material

True Plastic Strain (in/in)	True Stress (MPa)	True Stress (psi)
0.0000	339.22	49,200
0.0060	339.91	49,300
0.0120	340.60	49,400
0.0200	380.81	55,231
0.0280	406.93	59,021
0.0400	437.00	63,382
0.0550	466.10	67,602
0.0700	488.44	70,842
0.0850	505.23	73,278
0.1000	519.47	75,343
0.1150	531.53	77,092
0.1300	542.24	78,646
0.1450	552.06	80,070
0.1600	560.20	81,250
1.0000	970.33	140,734

After defining a plastic stress-strain response for each material, the results of the tensile tests were used to develop a triaxiality-based damage initiation envelope. The damage initiation envelopes for each section were developed using the “Quick Calibration” method described by Lee and Wierzbicki [10]. In the case of the end sheet and baffle samples, one of the required inputs for the Quick Calibration method, final thickness of the gage, was unfortunately not measured. The final thicknesses were therefore estimated using the FE models of the samples in an iterative process. The damage initiation envelope for the side sheet samples with the measured final thicknesses were also scaled in a similar fashion by applying a scaling factor so that all of the damage initiation envelopes could be created in a similar manner.

The resulting damage initiation envelopes for each post-test material is shown in Figure B12, alongside the constant strain-to-failure envelope that was used in the pre-test modeling. The difference between the damage initiation envelope for the side sheet material when compared with the end sheet and baffle material can be attributed to the use of shell elements in modeling the side sheet, whereas solid elements were used in modeling the end sheet and baffle samples.

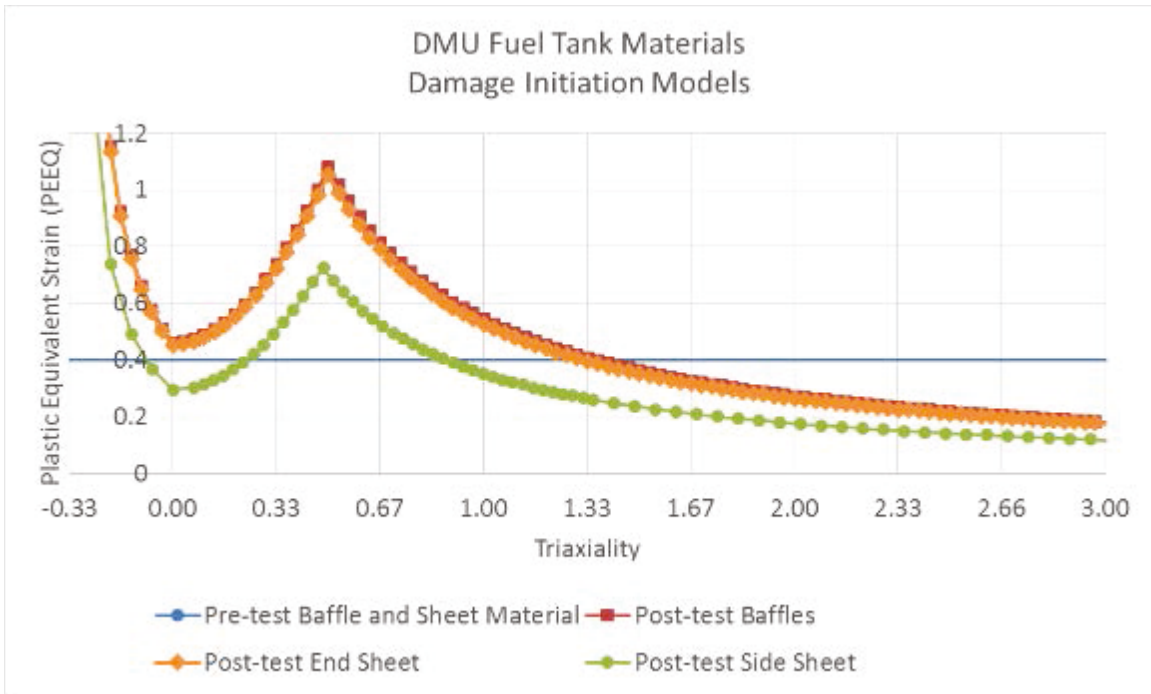


Figure B12. Damage Initiation Envelopes for Post-Test Materials

The final material parameter that was defined in the post-test FE model was the damage progression value. Once the combination of plastic equivalent (PEEQ) strain and triaxiality at a section point exceeded the damage initiation envelope for the material applied to that element, the element would begin to lose its load-carrying ability. The Abaqus software includes several parameters that can be defined to describe how the damage progresses from initiation to the element being fully removed. For each of the three materials for which sample data was measured, a linear energy-based damage progression was found to give the best agreement between the tensile sample tests and FE models with respect to the softening observed after the onset of necking as well as the final reduction in area. The magnitude of the damage progression was found iteratively by comparing the FE results with test measurements. The values used in the post-test FE models are shown in Table B5 for each material.

Table B7. Values of Damage Progression Used in Post-Test FE Models

	Progression Type	Progression Shape	Progression Value (N-mm/mm ²)
End Sheet	Energy	Linear	3,000
Baffles	Energy	Linear	5,000
Side Sheet	Energy	Linear	3,000

It is important to note that the progression values used in this model were optimized so that the resulting engineering stress-strain curve from the FE models matched the tensile test results. There are multiple outputs that could have been compared to iteratively select the progression value, such as toughness (area under the stress-strain curve), strain at fracture, final thickness, or final width. Future work may be considered that uses an automated methodology designed to optimize a weighted combination of these outputs to better understand how comparing different sample measurements affect the agreement between other outputs.

Appendix C – Test Data

Figures C1 through C12 contain raw and filtered test data. The raw accelerations measured on different locations on the impact cart were processed as follows for this test. The test data from -1 second to 4 seconds on each channel were averaged, and this value was subtracted from the test measurements in order to remove any initial offsets in the data. Each channel was then filtered to CFC 60, using the procedures given in SAE J211 [7].

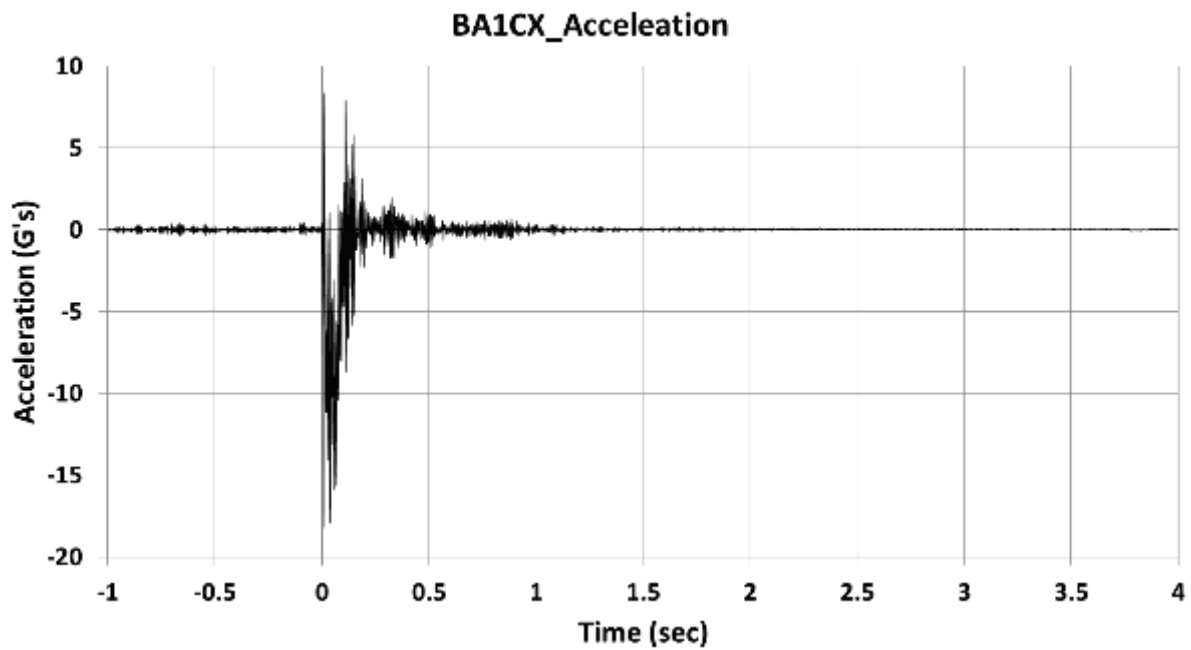


Figure C1. BA1CX Accelerometer Data

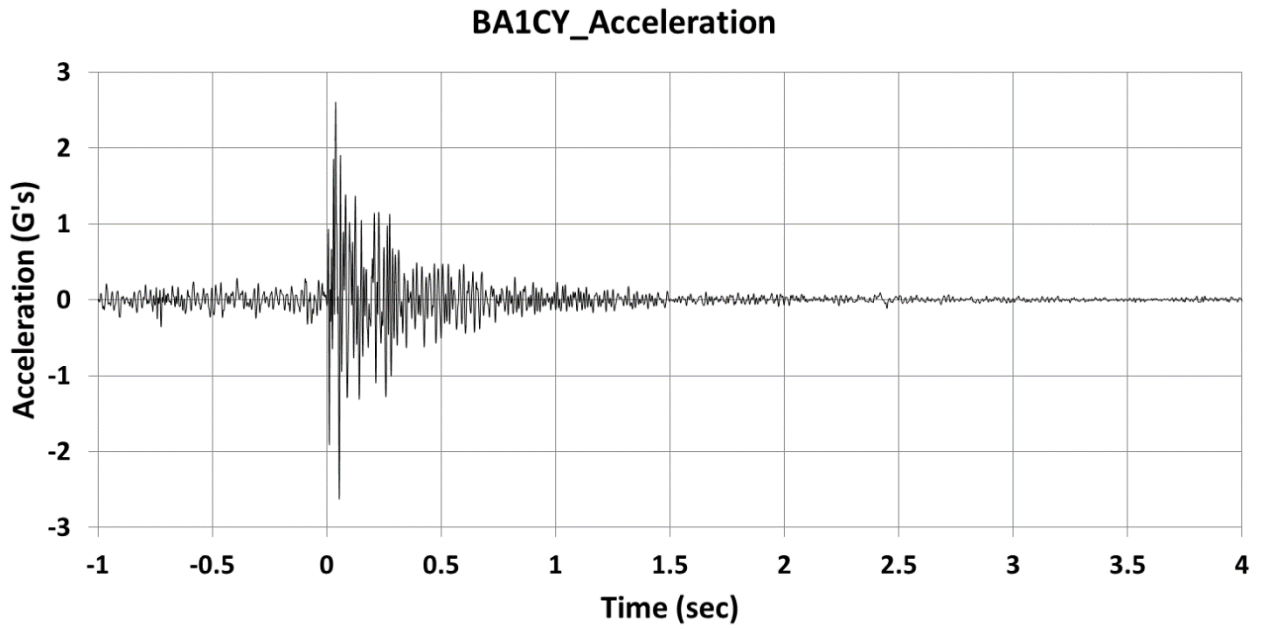


Figure C2. BA1CY Accelerometer Data

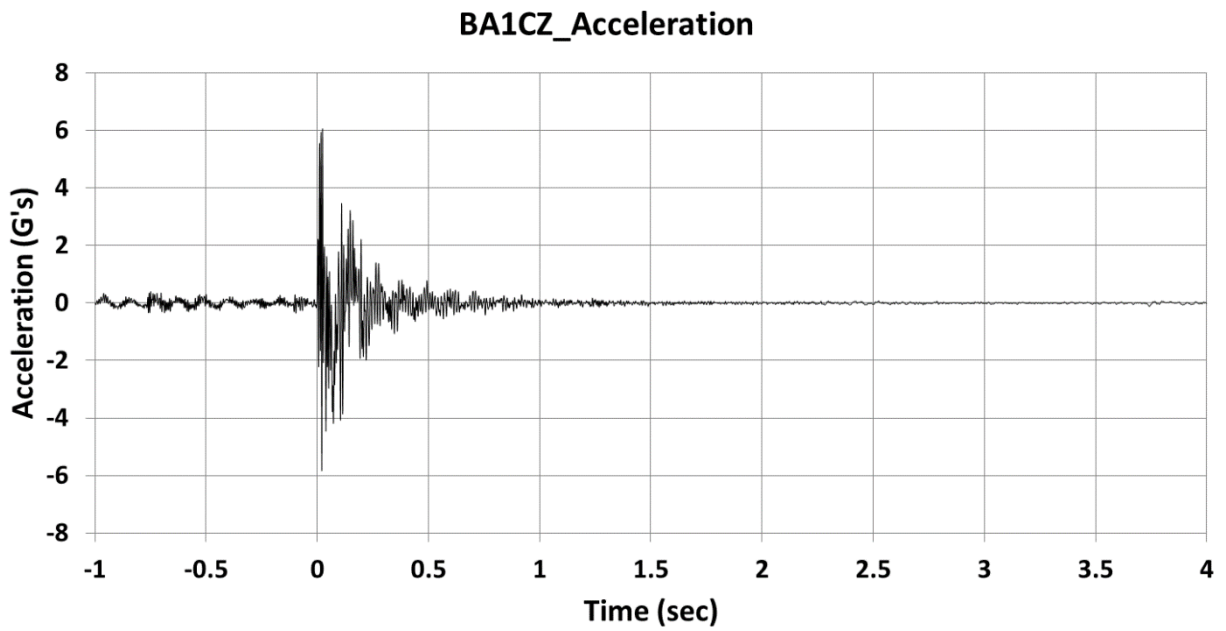


Figure C3. BA1CZ Accelerometer Data

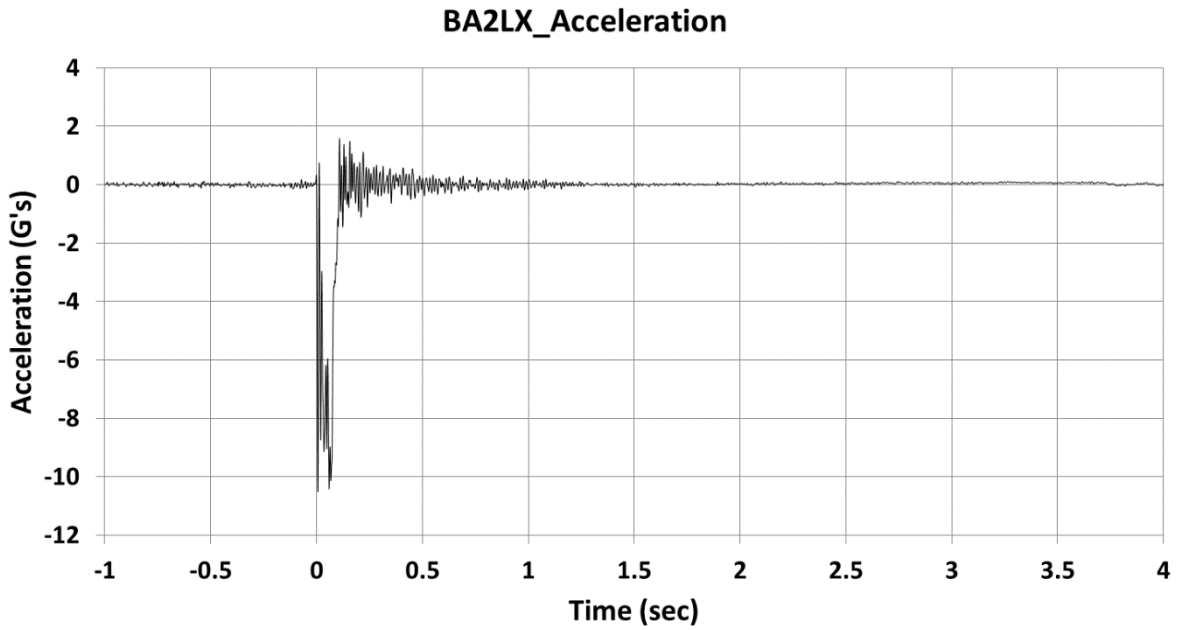


Figure C4. BA2LX Accelerometer Data

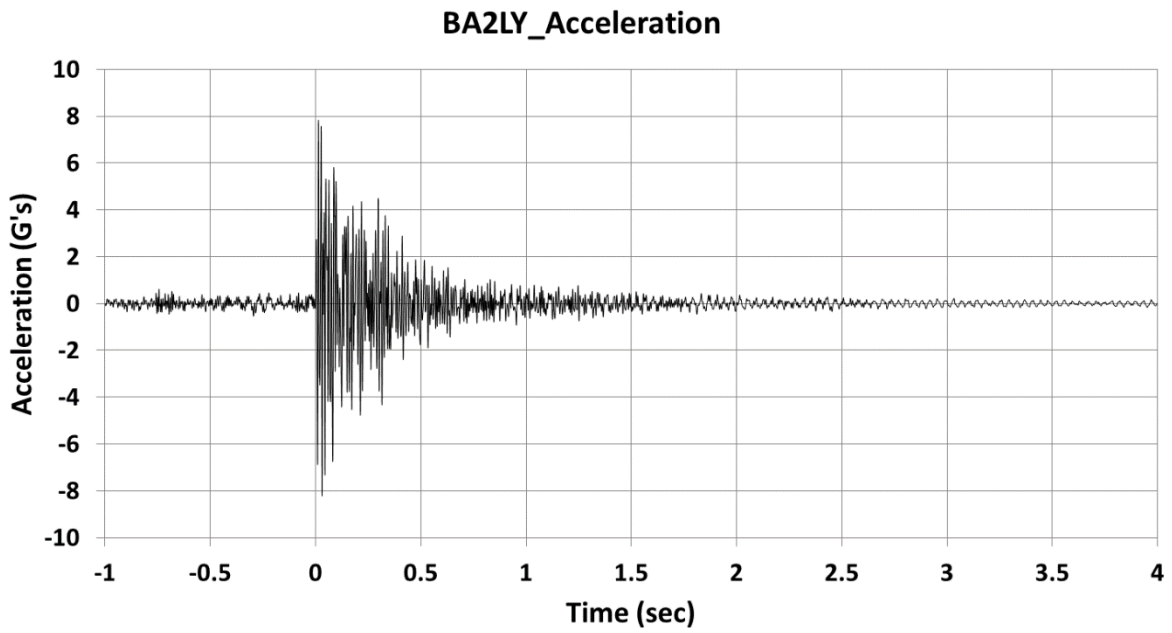


Figure C5. BA2LY Accelerometer Data

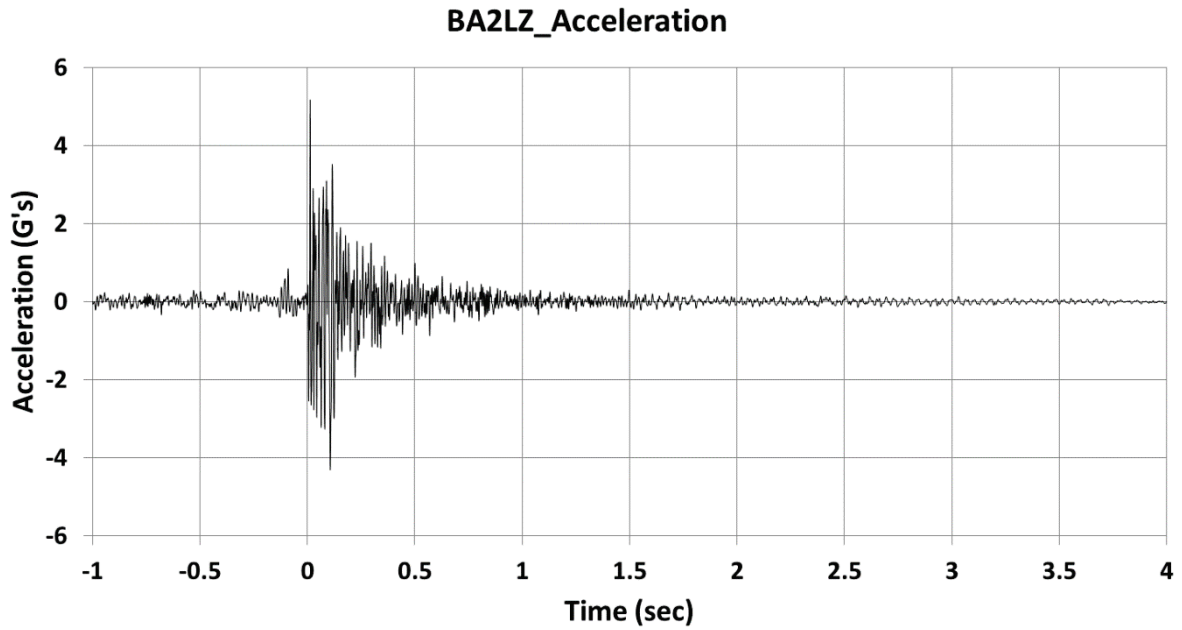


Figure C6. BA2LZ Accelerometer Data

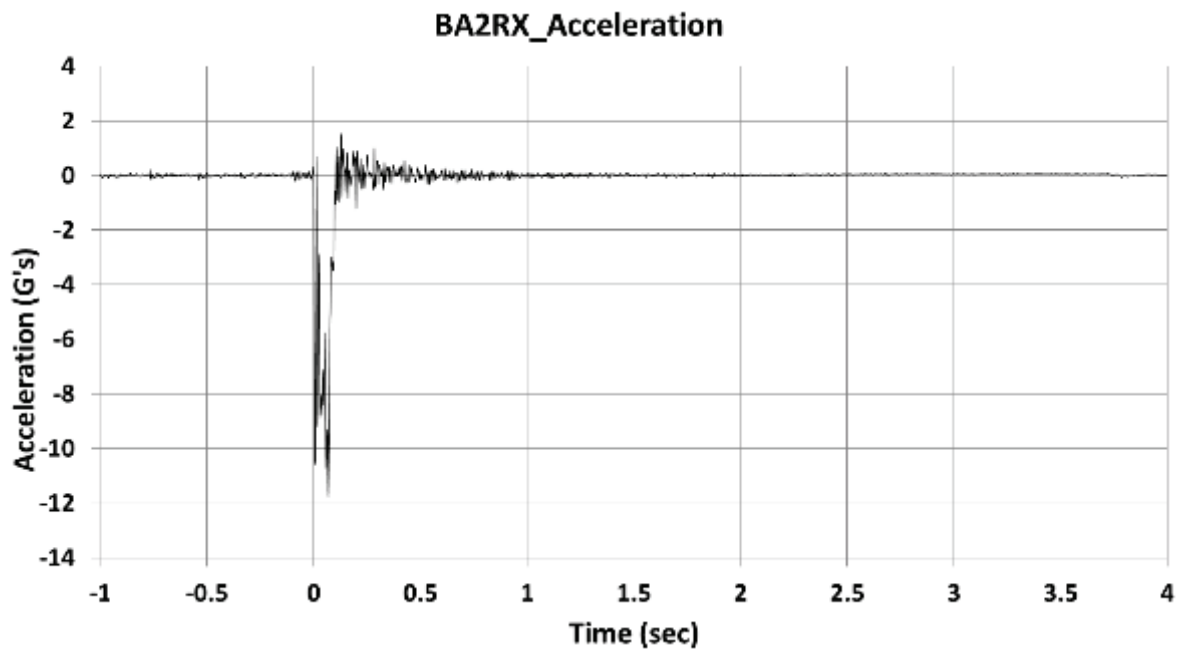


Figure C7. BA2RX Accelerometer Data

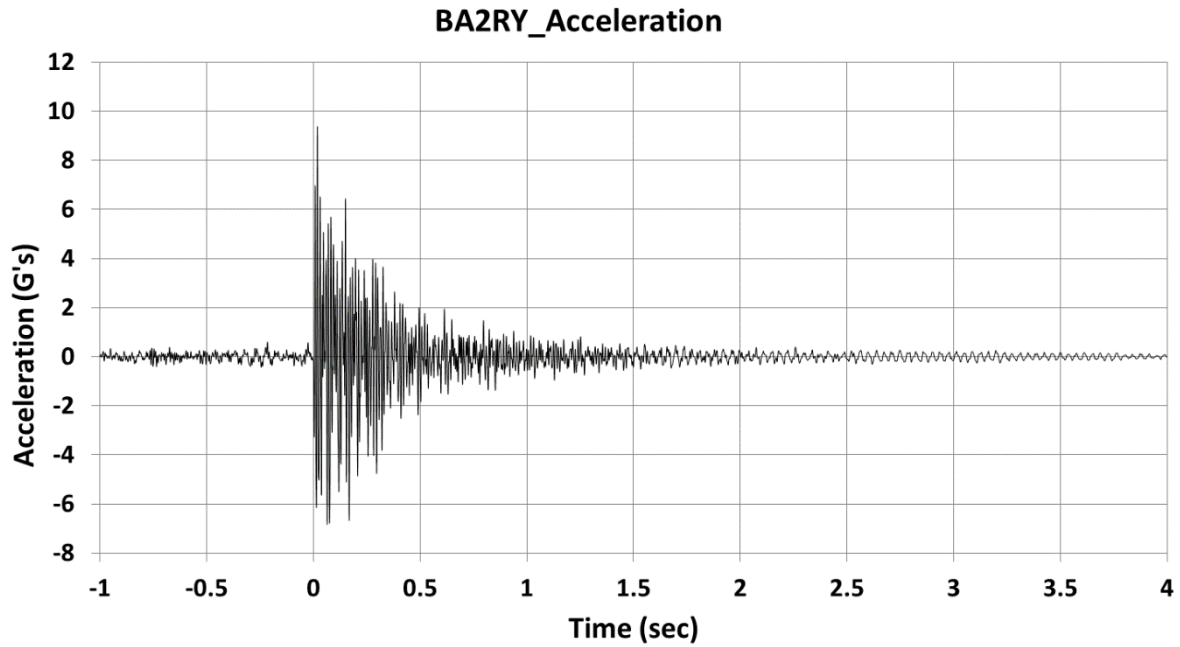


Figure C8. BA2RY Accelerometer Data

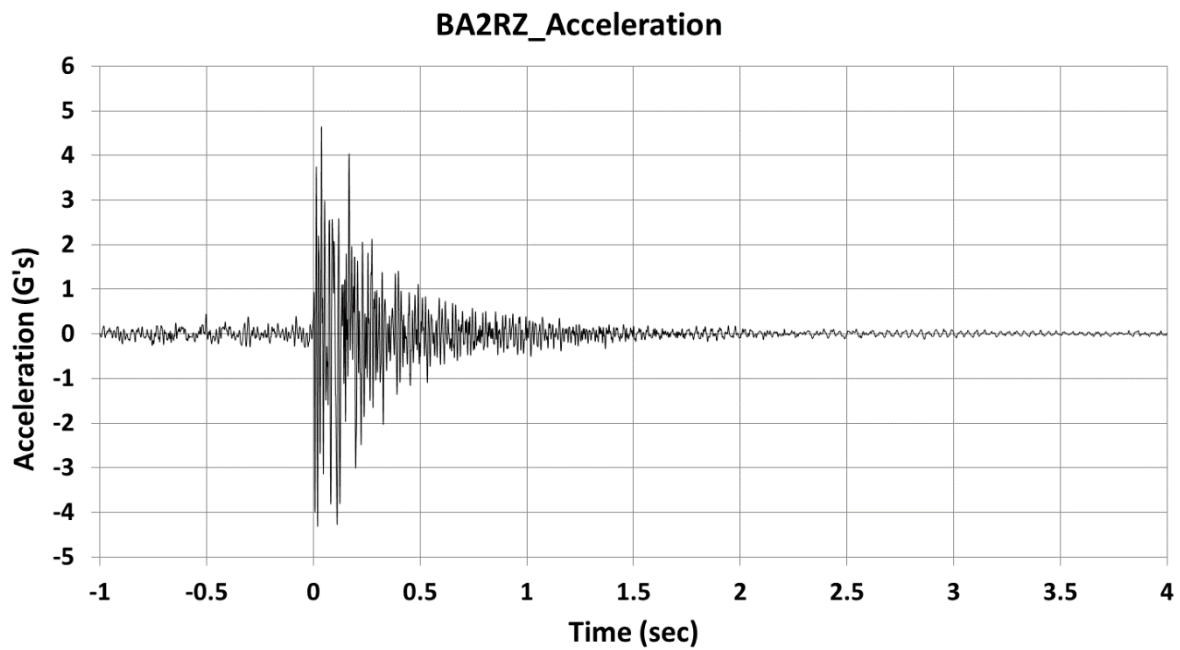


Figure C9. BA2RZ Accelerometer Data

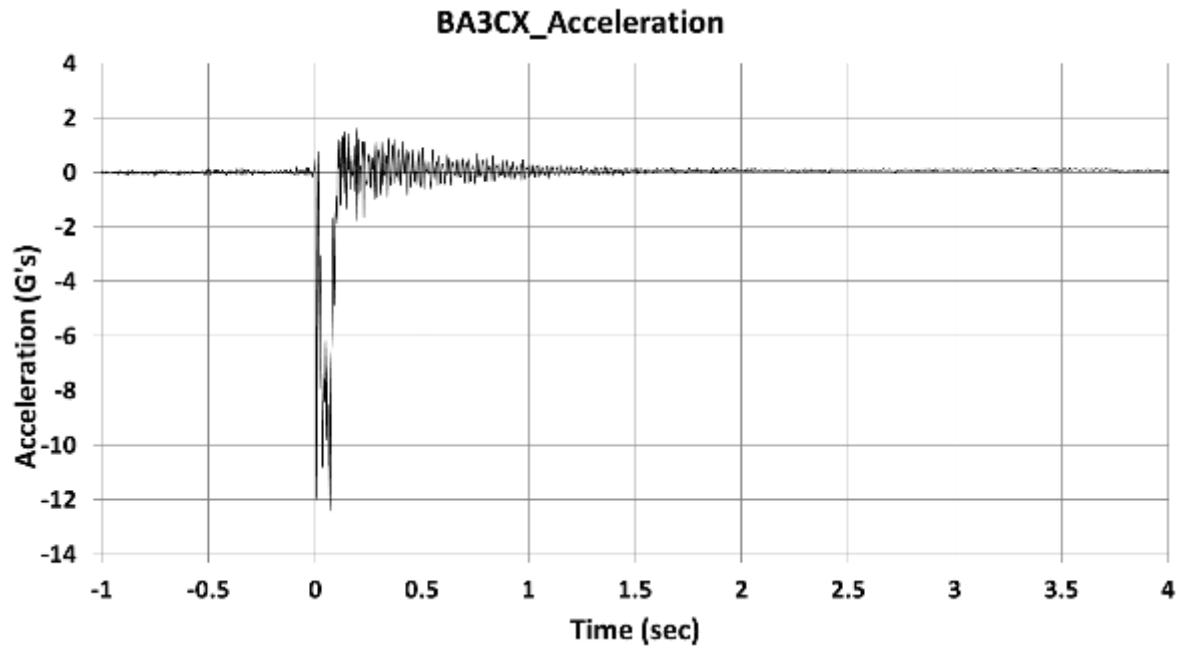


Figure C10. BA3CX Accelerometer Data

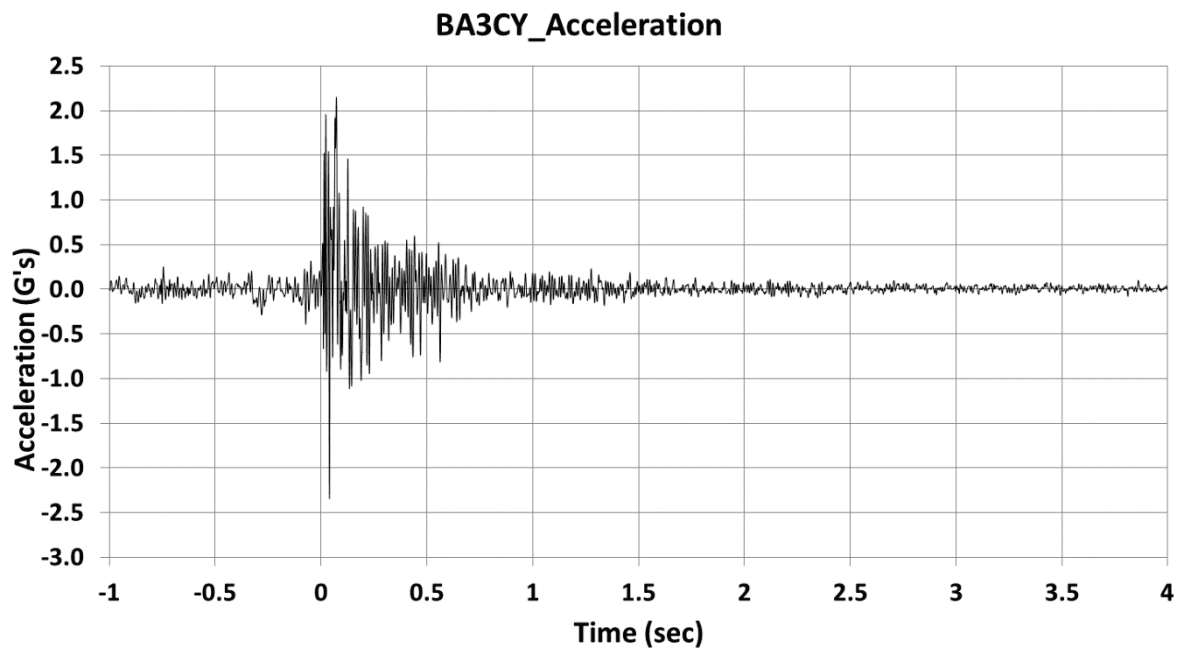


Figure C11. BA3CY Accelerometer Data

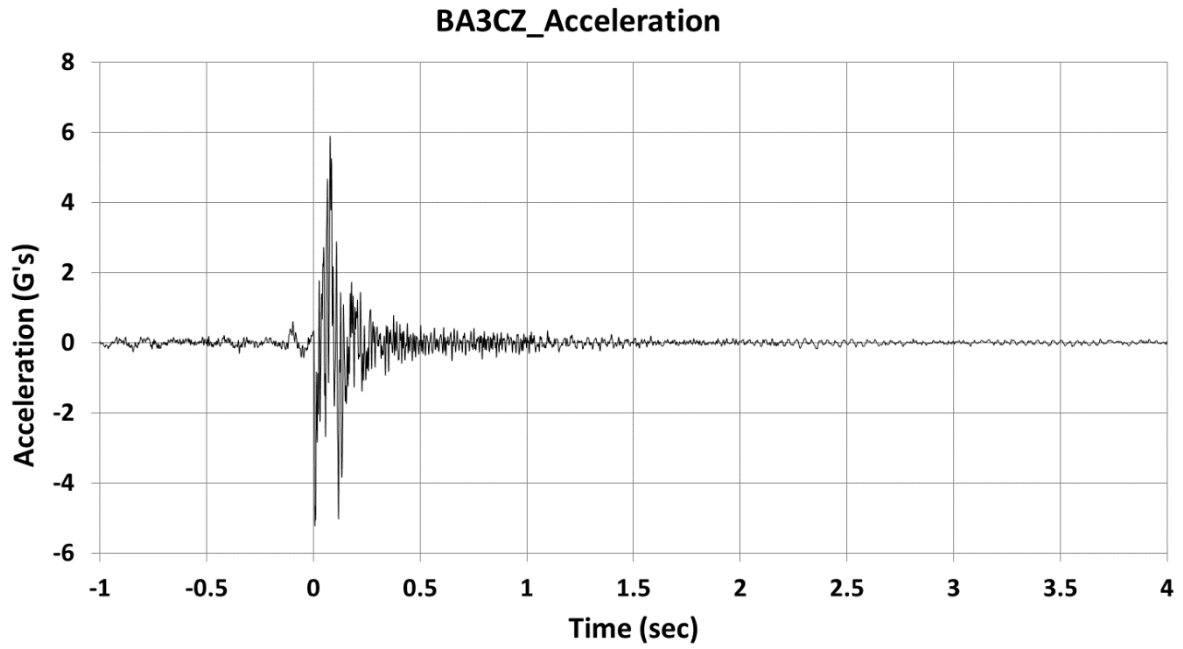


Figure C12. BA3CZ Accelerometer Data

Appendix D – Comparison Between Test Data and Finite Element Analysis Results

This appendix contains comparisons between the filtered test data and FEA results for the longitudinal acceleration quantities as obtained through the onboard accelerometers in the case of test data or derived from acceleration measurements at corresponding locations for FEA results involving a deformable impact cart. For each acceleration-time history, velocity, and position histories are also compared between test and FEA. Velocity-time data were obtained by integrating the filtered acceleration-time history, and setting the speed at $t=0$ equal to the average time obtained by the speed trap measurements. Finally, displacement-time data were obtained by integrating the velocity-time data and setting the displacement at $t=0$ equal to 0 inch.

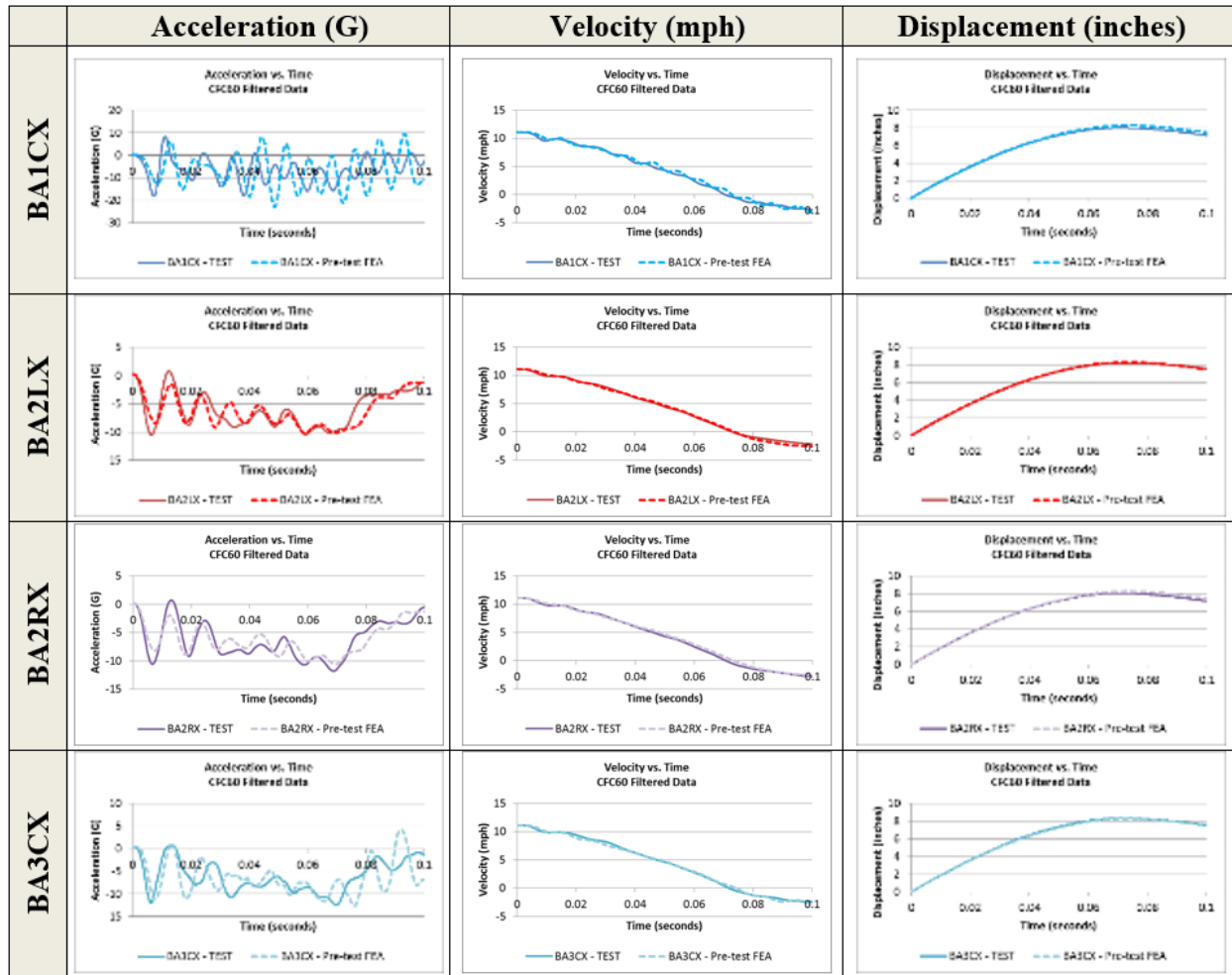


Figure D1. Pre-Test Model: Impact Speed: 11.2 mph (Test), 11.1 mph (FEA)

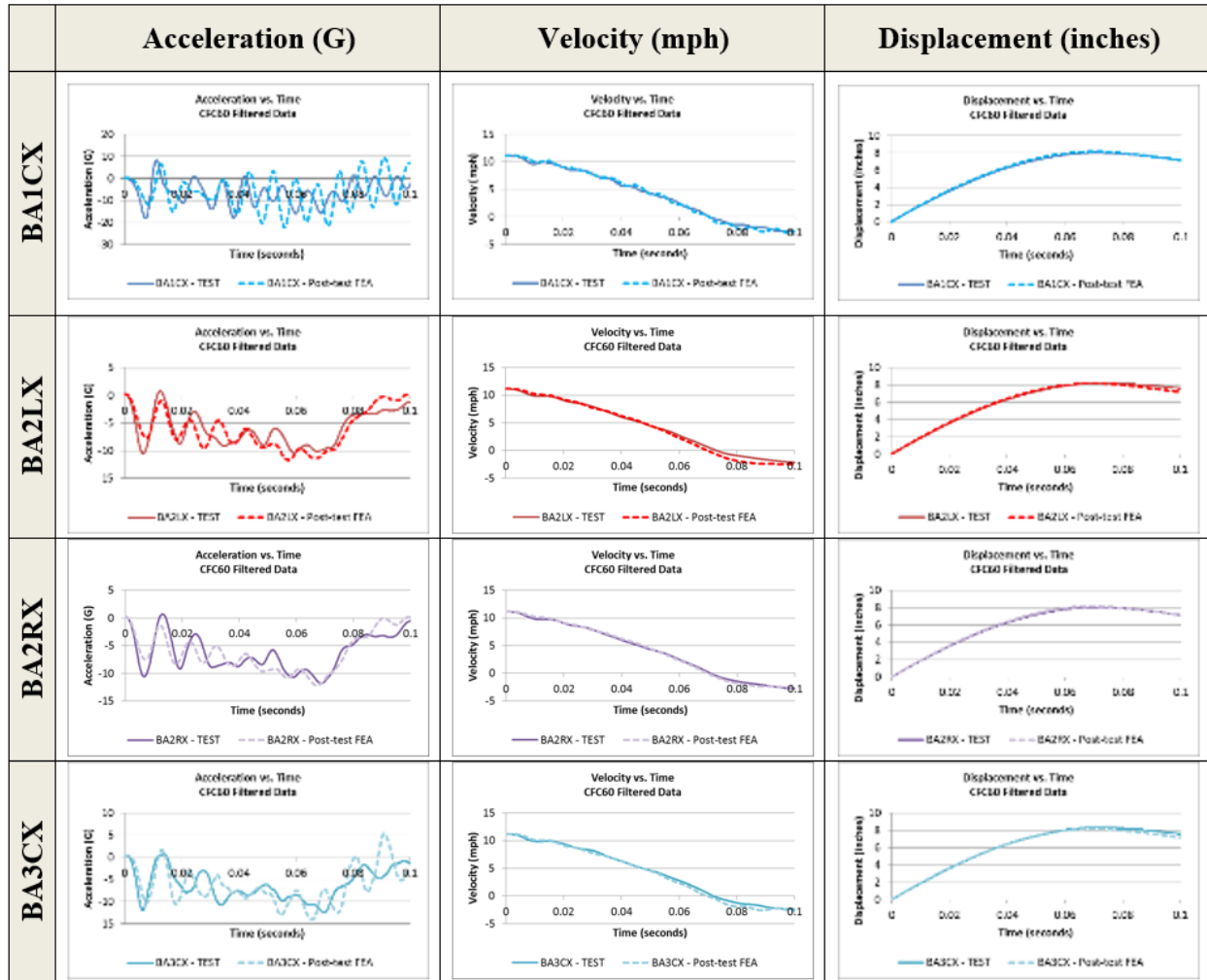


Figure D2. Post-Test Model: Impact Speed: 11.2 mph (Test and FEA)

Abbreviations and Acronyms

AAR	Association of American Railroads
APTA	American Public Transportation Association
CFC	Channel Frequency Class
CAD	Computer Aided Design
CFR	Code of Federal Regulations
DMU	Diesel Multiple Unit
DOF	Degrees of Freedom
FE	Finite Element
FEA	Finite Element Analysis
FRA	Federal Railroad Administration
LIDAR	Light Detection and Ranging
MBTA	Massachusetts Bay Transportation Authority
PEEQ	Plastic Equivalent
TTC	Transportation Technology Center
TTCI	Transportation Technology Center, Inc.
UTS	Ultimate Tensile Strength
Volpe	Department of Transportation's John A. Volpe National Transportation Systems Center